AD-A085 886 ILLINOIS UNIV AT URBANA-CHAMPAIGN COORDINATED SCIENCE LAB F/6 17/9
QUANTIZATION EFFECTS ON DIGITAL MTI.(U)
JAN 80 Y KWONG
UNCLASSIFIED R-868 DAAG29-78-C-0016 NL

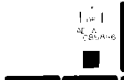

END
DATE FILMED
8-80
DTIC

REPORT R-968 JANUARY, 1980 UILU-ENG 80-2201

CSL COORDINATED SCIENCE LABORATORY

LEVEL II

12

# QUANTIZATION EFFECTS ON DIGITAL MTI



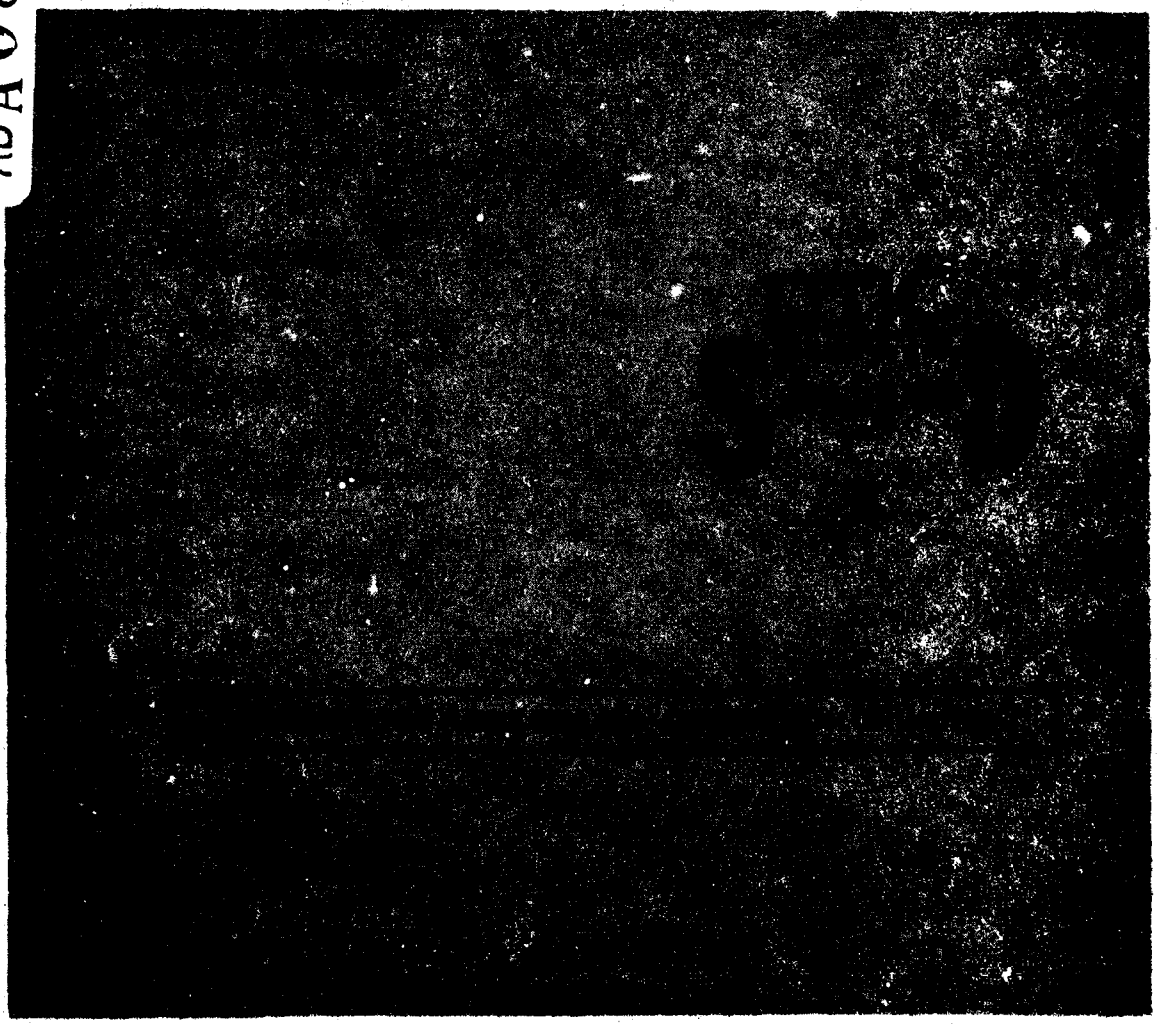



UNIVERSITY OF ILLINOIS - URBANA, ILLINOIS

UNCLASSIFIED

SECURITY CLASSIFICATION OF THIS PAGE (When Data Entered)

| REPORT DOCUMENTATION PAGE | READ INSTRUCTIONS BEFORE COMPLETING FORM |
|---|---|
| 1. REPORT NUMBER | 2. GOVT ACCESSION NO. AD-A085 886 / 3. RECIPIENT'S CATALOG NUMBER |
| 4. TITLE (and Subtitle) QUANTIZATION EFFECTS ON DIGITAL MTI | 5. TYPE OF REPORT & PERIOD COVERED Technical Report |
| | 6. PERFORMING ORG. REPORT NUMBER R-868, UILU-ENG-80-2201 |
| 7. AUTHOR(s) Yu-Hong Kwong | 8. CONTRACT OR GRANT NUMBER(s) DAAG-29-78-C-0016, N00014-79-C-0424 |
| 9. PERFORMING ORGANIZATION NAME AND ADDRESS Coordinated Science Laboratory, University of Illinois at Urbana-Champaign, Urbana, Illinois 61801 | 10. PROGRAM ELEMENT, PROJECT, TASK AREA & WORK UNIT NUMBERS |
| 11. CONTROLLING OFFICE NAME AND ADDRESS Joint Services Electronics Program | 12. REPORT DATE 1979 |
| | 13. NUMBER OF PAGES 61 |
| 14. MONITORING AGENCY NAME & ADDRESS (if different from Controlling Office) | 15. SECURITY CLASS. (of this report) UNCLASSIFIED |
| | 15a. DECLASSIFICATION/DOWNGRADING SCHEDULE |

16. DISTRIBUTION STATEMENT (of this Report)

Approved for public release; distribution unlimited

17. DISTRIBUTION STATEMENT (of the abstract entered in Block 20, if different from Report)

18. SUPPLEMENTARY NOTES

19. KEY WORDS (Continue on reverse side if necessary and identify by block number)

Radar Digital MTI, Quantization, Companding

20. ABSTRACT (Continue on reverse side if necessary and identify by block number)

The processing of digital signals is rapidly approaching a dominant role in both communication and radar systems. However, the physical origin of many information-bearing signals is intrinsically analog and continuous-time in nature. Therefore, an effective interface between the analog and digital worlds is of significant importance in modern signal-processing. Very often the quality of analog-to-digital (A/D) conversion is the critical limiting factor in over-all system performance.

DD FORM 1 JAN 73 1473 EDITION OF 1 NOV 65 IS OBSOLETE

UNCLASSIFIED

SECURITY CLASSIFICATION OF THIS PAGE (When Data Entered)

UILU-ENG 80-2201

# QUANTIZATION EFFECTS ON DIGITAL MTI

by

Yu-Hong Kwong

This work was supported in part by the Joint Services Electronics Program (U.S. Army, U.S. Navy and U.S. Air Force) under Contracts DAAG-29-78-C-0016 and N00014-79-C-0424.

# QUANTIZATION EFFECTS ON DIGITAL MTI

BY

YU-HONG KWONG

B.S., Columbia University, 1977

THESIS

Submitted in partial fulfillment of the requirements
for the degree of Master of Science in Electrical Engineering
in the Graduate College of the
University of Illinois at Urbana-Champaign, 1980

Thesis Adviser: Professor H. Vincent Poor

Urbana, Illinois

ACKNOWLEDGMENTS

I would like to express my deep gratitude to Professor H. Vincent Poor for his valuable advice, guidance and assistance, and to Mrs. Phyllis A. Young for her excellent typing of the thesis.

TABLE OF CONTENTS

# 1. INTRODUCTION

The processing of digital signals is rapidly approaching a dominant role in both communication and radar systems. However, the physical origin of many information-bearing signals is intrinsically analog and continuous-time in nature. Therefore, an effective interface between the analog and digital worlds is of significant importance in modern signal-processing. Very often the quality of analog-to-digital (A/D) conversion is the critical limiting factor in over-all system performance.

Quantization, the essential mechanism of A/D conversion, begins with the availability of input values ranging from $-\infty$ to $+\infty$. The quantizer replaces each of these input values with a prechosen output value. The key feature is that each output value is one of a finite set of real numbers. Hence, a symbol from a finite alphabet can be used to represent and identify the particular output values that occur. Intuitively, a different n-bit binary word can then be associated with each output value if the set of output values contains no more than $2^n$ members.

The moving target indicator (MTI) is a processor required in most search radars to separate moving targets from stationary clutter. Nevertheless, the implementation of an MTI by analog means has been hindered somewhat because of the instability problems incorporated in an MTI system. Quantization of an MTI system with digital means is one of the possible remedies to these problems. Because the characteristics of a quantizer are governed by the choice of the number of output levels and the spacings and step sizes of these levels, the performance of an MTI with a quantizer will depend solely on the above parameters. It is the effect of these parameters on the digital MTI that will be discussed in this thesis.

# 2. A BRIEF INTRODUCTION TO MOVING-TARGET INDICATION

One of the basic requirements for present-day tactical radars is desirable performance in a heavy clutter environment. This requirement often leads to a radar system approach which utilizes a moving target indicator (MTI) to extract moving targets from the clutter background. MTI systems operate by virtue of the Doppler spectral differences between returns from moving targets and clutter. For instance, if the target is moving relative to the clutter background, the MTI can be applied to filter out the undesired clutter return by exploiting the differential Doppler frequency shift produced by the relative target to clutter radial motion [1].

## 2.1 Historical Development

In early radars, most MTI systems were implemented by using analog techniques. In the 1950's, MTIs were primarily of the analog single canceller type that used a quartz ultrasonic delay line to delay the radar return by a time corresponding to the radar's pulse repetition frequency (PRF). The desired MTI effect was produced by subtracting the delayed return from the present return. More advanced MTI systems employed a double canceller that was formed by connecting two single cancellers in cascade. This configuration not only produced a more desirable transfer function, but also compensated for unbalances in each of the individual cancellation circuits. Multiple cancellers are discussed and analyzed

by Emerson [2]. However, it has been shown that the added complexity of the multiple cancellers offers little advantage in terms of performance over their counterparts. Thus the inability to control the delay time and the system gain by analog means have made it hard to enhance the analog MTI to operate toward the theoretical limit.

Also during the 1950's, attention had been focused on methods to implement better MTI operation within the existing hardware constraints. It was found that applying feedback around a double canceller type MTI allowed excellent control of the shape of both the passband and rejection band of the MTI [3,4,5]. However, when this technique was incorporated into operational radars, a significant problem was observed: any asynchronous interference present caused a transient that circulated around the velocity shaped canceller for many PRF periods resulting in unacceptable operation. Hence current MTI design practice tends to use nonrecursive type MTI filters wherever possible [6,7,8,9] to take advantage of their superior transient response.

More recently, because of the availability of the technology of semiconductor electronics and integrated digital devices, microelectronic range-gated filter [2] and digital MTIs have also been implemented. The range-gated filter MTI, as the name implies, range-gates the coherent MTI signal into a filter that separates the target from the clutter. McAulay [10] has shown that the optimum MTI processor is achieved when a clutter filter is cascaded with a bank of contiguous Doppler filters matched to the target spectrum. This implementation simultaneously

performs Doppler filtering and coherent integration, but has the disadvantage that a large number of filters is required. On the other hand, the digital MTI is basically a digital implementation of the analog MTI. In fact, digital techniques are not only practical but they are essential to meet the present day tactical requirements of light weight, small volume, high availability, and near-optimum system performance at a reasonable cost. Hence, the relative high cost of range-gated filter MTIs and the development of low cost digital components results in a general preference for digital MTIs.

The MTI problem for surface-based radars is less complex than that for airborne radars [2,11]. The complications in airborne radars arise primarily because of the clutter spectral spreading and translation effects caused by platform motion in addition to the aircraft-to-surface geometry. There are two general approaches for solving the airborne MTI (AMTI) clutter problem. The first is generally referred to as a pulse Doppler radar. Pulse Doppler radars are used for airborne interceptor (AI) radars where "look down" in heavy clutter is required. One application of this technique is to the AWACS EC-121 airborne radar [12]. The other approach for solving the AMTI radar clutter problem is to remove the effects of aircraft motion by antenna design and signal processing. Once the platform motion effects are removed, the same signal processing techniques as used in the surface MTIs are applicable. Rhys and Andrews [13] has a detailed description of this type of system. Application of this technique is to the E2-C airborne early warning (AEW) radar.

## 2.2 Clutter Modeling

Before we analyze the performance of the MTI radars, the characteristic of the clutter environments should be discussed. Since an MTI system might perform better in one clutter environment than in another, a clutter model assumption is implicit in the design or analysis of the system.

Ideally, the model used should accurately reflect the clutter process in a realistic manner. Practically, the clutter data base is rarely adequate to achieve this objective, and the art of modeling the clutter involves a compromise between accurate representation and analytic convenience. The following is a brief overview of the various clutter models used commonly in the design or analysis of the MTI:

(i) The Gaussian (Rayleigh Envelope) Clutter Model

The Gaussian or Rayleigh envelope clutter model is applicable to distributed clutter that is returned from a spatially continuous distribution of scatterers with no subset of scatterers predominating. This type of clutter is usually associated with weather clutter, chaff, sea clutter observed with a low resolution radar (pulse width $> 0.5\ \mu$ sec) or with a high-resolution radar at high grazing angles ($\varphi > 5^{o}$) and land clutter observed for high grazing angles ($\varphi > 5^{o}$) over undeveloped terrain.

The random clutter process is represented at the clutter carrier frequency ($f_c$) as

$$c_t = x_t \cos \omega_c t - y_t \sin \omega_c t \qquad (2.1)$$

where $x_y$ and $y_t$ are zero mean, identically distributed, low pass,

independent normal processes with variance $\sigma^2$. The clutter process $c_t$ is strict-sense stationary and hence its characteristics are independent of the time origin.

The power spectral density associated with the randomly fluctuating portion of the clutter cross-section is usually assumed to be Gaussian shaped in that it is the result of several independent effects. The power spectral density of the power envelope is given by

$$S_p(f) = \frac{P_c}{\sqrt{2\pi\sigma_f^2}} \exp[-f^2/2\sigma_f^2] \tag{2.2}$$

where $P_c$ is the clutter power and $\sigma_f$ is the standard deviation of the spectrum.

The autocorrelation function associated with the power envelope is given by

$$R_p(\tau) = P_c \exp[-\tau^2/2\sigma_\tau^2] \tag{2.3}$$

where $\sigma_\tau = 1/2\pi\sigma_f$.

The normalized autocorrelation function is then

$$\rho_c(\tau) = R_p(\tau)/P_c = \exp[-\tau^2/2\sigma_\tau^2] \tag{2.4}$$

(ii) The Rician Clutter Model

The Rician clutter model is similar to the Gaussian model except that a predominant steady scatterer (S) is added to the distributed clutter.

The random clutter process is represented by

$$C_t = (S+x_t) \cos \omega_c t - y_t \sin \omega_c t \quad .$$

The autocorrelation function for the in-phase process and Gaussian shaped distributed clutter is

$$R(\tau) = P_o[m^2 + \exp(-\tau^2/2\sigma_\tau^2)]$$

where $P_o$ is the distributed power and $m^2 = S^2/P_o$.

The resulting power spectral density is

$$S(f) = m^2 P_o \delta(f) + P_o \exp(-f^2/2\sigma_f^2)/\sqrt{2\pi\sigma_f^2}.$$

(iii) The Log-Normal Clutter Model

The log-normal clutter model is associated with high resolution (pulse width < .5 sec) sea-clutter data, where the sea clutter is observed at grazing angles ($\varphi < 5^o$); and ground clutter observed at low grazing angles.

The random clutter process is represented by

$$c_t = \sqrt{x_t^2 + y_t^2} \cos(\omega_c t + \varphi_c)$$

where $\varphi_c$ is a uniformly distributed random variable.

The log normal ($Z_t$) variable is related to the Gaussian variable ($x_t$) by a nonlinear function, A exp(·), where A is a constant and in which

$$E(Z_t) = A \exp[\frac{R_x(0)}{2}]$$

$$R_Z(\tau) = A^2 \exp[R_x(0) + R_x(\tau)]$$

$$C_Z(\tau) = A^2 \exp[R_x(0)][\exp[R_x(0)]-1]$$

where $R_x(\tau)$: autocorrelation function (ACF) of the Gaussian variable

$R_Z(\tau)$: ACF of the log-normal variable

$C_Z(\tau)$: covariance function of the log-normal variable.

(iv) The Weibull Clutter Model

The Weibull clutter model is used to model both land and sea clutter and offers the potential to accurately represent the real clutter distribution over a much wider range of conditions than either the log-normal or Gaussian model. Szajnowski [14] has the derivation of the correlation properties of the Weibull clutter model. He showed that the correlation function of the Weibull clutter process is related to that of the Gaussian clutter process. Moreover, the Weibull ($W_t$) variable, which is governed by two parameters p and q, is related to two independent Gaussian variables $x_t$ and $y_t$ such that

$$W_t = (x_t^2 + y_t^2)^{1/p}$$

where $x_t$ and $y_t$ are zero-mean identically distributed Gaussian variables with variance $\sigma^2$, p is the sample parameter and q is the scale parameter related to $\sigma^2$ by $q = (2\sigma^2)^{1/p}$. The mean $E\{W_t\}$ and the variance $\sigma_W^2$ of the Weibull variable are

$$E\{W_t\} = (2\sigma^2)^{1/p}\,\Gamma(1 + 1/p)$$

$$\sigma_W^2 = (2\sigma^2)^{2/p}\{(1 + 2/p) - \Gamma^2(1 + 1/p)\}$$

where $\Gamma(\cdot)$ is a gamma function.

Of the above, the simplest clutter model is the Gaussian model whereby the random clutter process is represented as a Gaussian process which is completely specified by its mean and correlation function. At present, analytical techniques are not available to determine the performance of MTI systems in the presence of non-Gaussian clutter. The principle method of attacking this type of problem is through a Monte Carlo computer simulation in which the actual MTI system is exercised by applying statistical samples of the postulated clutter and target processes. For this reason, the Gaussian model has been used exclusively in the MTI analysis. Henceforth, we shall choose the Gaussian model instead of the others as the clutter model throughout the remainder of the thesis.

## 2.3 MTI System Performance

The ultimate measure of the MTI system performance, i.e., the capability of the MTI to separate moving targets submerged in the clutter, does not depend on power considerations alone. The following performance criteria are seen most often:

(i) Clutter Attenuation (CA)

This criterion is defined as the ratio of the power in the clutter before Doppler filtering to the power in the clutter after Doppler filtering, with the output clutter power normalized to unity gain for uncanceled signals; i.e.,

$$CA = \frac{\int_0^\infty S_c(\omega)\,d\omega}{\int_0^\infty S_c(\omega)\,|H(\omega)|^2\,d\omega}$$

where $S_c(\omega)$ is the clutter power spectral density and $H(\omega)$ is the MTI filter transfer function.

(ii) Subclutter Visibility (SCV)

Subclutter visibility is defined as the ratio at the input of the Doppler filter of clutter power to moving target power to produce equal Doppler filter outputs. Specifically,

$$SCV = \frac{\int_0^\infty S_T(\omega-\omega_d)\,|H(\omega)|^2 d\omega}{\int_0^\infty S_c(\omega)\,|H(\omega)|^2 d\omega} \quad ; \; P_c = P_T$$

where $S_T(\omega-\omega_d)$ is the target power spectral density. The SCV equation is usually evaluated at $\omega_d$ equal to an optimum speed target; i.e., a target whose Doppler frequency is one-half the radar's pulse repetition frequency. However, it is more fundamental to evaluate the SCV at the target speeds of interest.

(iii) Improvement Factor (or Reference Gain) (I)

This criterion is found by comparing the input signal-to-clutter ratio to the MTI output signal-to-clutter ratio for targets distributed uniformly over the radial velocity spectrum.

$$I = \frac{(P_s/P_c)_o}{(P_s/P_c)_i} \quad ; \text{ average over all possible target Doppler frequencies}$$

(iv) MTI Gain

The gain of an MTI is defined as the output of the Doppler filter when excited with a process whose spectral density corresponding to all velocities of interest is uniformly distributed.

$$\text{MTI gain} = \frac{\int_0^{\omega_{max}} |H_n(\omega)|^2 d\omega}{\omega_{max}}$$

where $\omega_{max}$ is the maximum Doppler frequency of interest, and $|H_n(\omega)|^2$ is the normalized power transfer function.

Clutter attenuation and subclutter visibility are equivalent criteria when target and clutter spectral shapes are similar and the response of the Doppler filter is unity for the targets under consideration. For single and double cancellers, this occurs for optimum-speed targets. The improvement factor provides a criterion for computing the average improvement in the signal-to-clutter ratio introduced by the canceller; whereas, MTI gain provides a criterion for comparing target responses of various MTI filters.

In general, the criterion that best represents the desired objective of the system should be selected. For example, consider an MTI surveillance requirement where the moving target is to be located by examining a display. The MTI system must reduce the ground clutter to a level consistent with the radar's noise level to keep the false alarms at a tolerable level, while allowing the detection of weak targets. For this type of situation, the clutter attenuation and the MTI gain are appropriate performance measures; the first relating to the false-alarm performance, the second to the ability to detect a variety of targets. As a second example, consider a combat surveillance radar whose function is to detect personnel whose velocities are 1 to 3

knots. The performance criterion of interest here is maximum subclutter visibility evaluated at 1 to 3 knots velocities. For our discussion, the quantization effects on the digital MTI are to be analyzed, the desirable performance measure in this case is the clutter attenuation since it is most sensitive to the errors introduced by the quantizer [15].

# 3. PERFORMANCE EXPRESSIONS FOR DIGITAL MTI

## 3.1 An Analytical Model for Digital MTI

The performance of analog MTI systems has been limited by problems in controlling the delay times and gains of such systems. However, these problems have been overcome by a digital MTI system which is basically a system with a quantizer being inserted at the input of the analog MTI system. In the following discussion, the previous works related to the quantization effects on the digital MTI will be reviewed; however, the primary emphasis will be on the single and double canceller MTIs.

Mathematically, the output y(t) of a single-canceller MTI is related to the input voltage x(t) by

$$y(t) = x(t) - x(t+D) \tag{3.1}$$

where D is the system delay; and similarly for the double canceller MTI, the output is

$$y(t) = x(t) - 2x(t+D) + x(t+2D) \tag{3.2}$$

Eqs. (3.1) and (3.2) are for linear MTIs. If a quantizer is inserted before MTI delay, then outputs of the single and double canceller digital MTIs are

$$y_Q(t) = x_Q(t) - x_Q(t+D) \tag{3.3}$$

and

$$y_Q(t) = x_Q(t) - 2x_Q(t+D) + x_Q(t+2D) \tag{3.4}$$

respectively, where $x_Q(t)$ is a quantized version of the input x(t).

The block diagrams for a single canceller MTI, a double canceller MTI and a digital MTI are shown in Figs. 3.1, 3.2, and 3.3, respectively.

## 3.2 Distortion Effects Due to Digitizing MTI

Before deriving the equations needed for the analysis of the MTI performance, we will examine the distortions introduced in the presence of a quantizer.

In digital MTI, the quantizer is the critical element of the design, as the ultrasonic delay line is to the analog MTI. Because of the presence of the quantizer, digitized input generates basically two types of distortion.

The first is the quantization noise that must be considered in addition to the usual noise encountered in the analog MTI. Brennan and Reed [16] first defined the output ratio, $R_o$, as the performance criterion of an MTI system, where

$$R_o = \frac{|E\{y_Q(t)|\text{signal present}\} - E\{y_Q(t)|\text{signal absent}\}|^2}{\text{var}\{y_Q(t)|\text{signal absent}\}}$$

The numerator is the square of the incremental digitized output voltage in the presence of a signal, and the denominator is the variance of the digitized output voltage in the presence of the clutter plus quantization noise. In general, the expectation of $y_Q(t)$ is zero in the absence of signal [16]. Thus $R_o$ is simplified to the form in which

$$R_o = \frac{|E\{y_Q(t)|\text{signal present}\}|^2}{E\{|y_Q(t)|^2|\text{signal absent}\}}$$

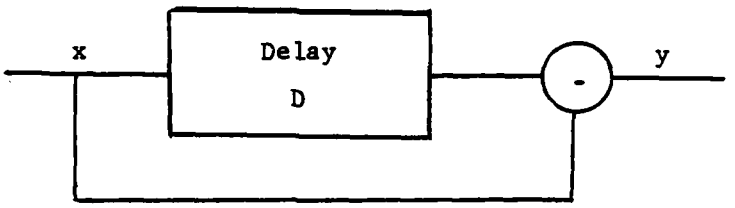


Figure 3.1. Single canceller MTI.

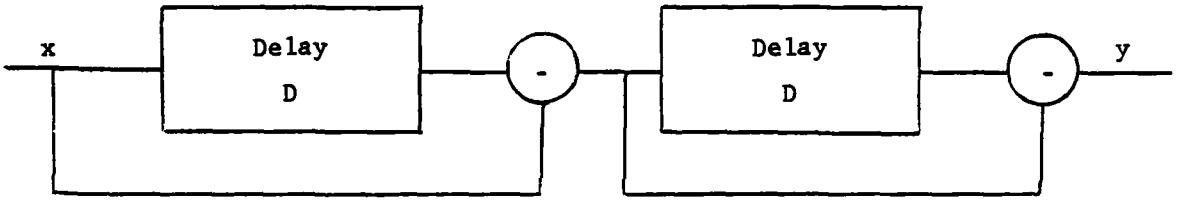


Figure 3.2. Double canceller MTI.

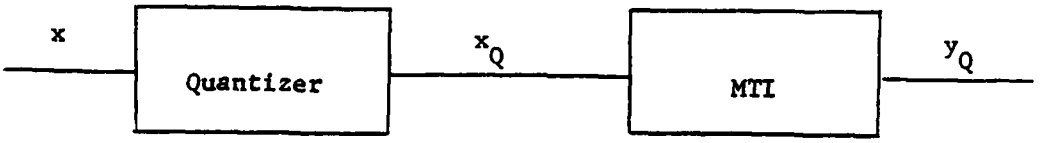


Figure 3.3. Digital MTI.

Brennan and Reed also identified a quieting effect due to correlation between quantization errors on successive pulses. For the case of interest, assume a uniform quantizer is utilized, the output ratio for a single canceller MTI is then (recall that we are assuming Gaussian statistics throughout)

$$R_o = \frac{(S_0-S_1)^2}{2\sigma_x^2[1-\rho_x(D)] + \frac{\Delta^2}{6}(1-Q)} \tag{3.5}$$

where $S_i = E\{X_Q(t+iD)|\text{signal present}\}$; $\sigma_x^2$ is the variance of the input process $x(t)$; $\rho_x(D)$ is the normalized correlation function of the input process $x(t)$; $\Delta$ is the quantization interval and Q is a quieting factor which is a measure of quieting due to correlation between quantization errors on two successive pulses; and mathematically Q is given by

$$Q = \frac{6}{\pi^2}\sum_{k=1}^{\infty}\frac{1}{k^2}\exp\{-4\pi^2k^2(\sigma_x/\Delta)^2[1-\rho_x(D)]\} \tag{3.6}$$

For a double canceller MTI, the output ratio is

$$R_o = \frac{(S_0 - 2S_1 - S_2)^2}{2\sigma_x^2[3-4\rho_x(D) + \rho_x(2D)] + \frac{\Delta^2}{2}(1-Q)} \tag{3.7}$$

In this case, the quieting factor is

$$Q = \frac{8}{\pi^2}\sum_{k=1}^{\infty}\frac{1}{k^2}\exp\{-4\pi^2k^2((\sigma_x/\Delta)^2[1-\rho_x(D)]\}$$

$$+ \frac{2}{\pi^2}\sum_{k=1}^{\infty}\frac{1}{k^2}\exp\{-4\pi^2k^2(\sigma_x/\Delta)^2[1-\rho_x(2D)]\} \tag{3.8}$$

Each of the denominators of Eqs. (3.5) and (3.7) contains two terms. The first is the residue clutter power in the absence of quantization noise, and the second is the noise power due to quantization. Without the quieting effect, as for the single canceller MTI, the second term simplifies to $\Delta^2/6$, which can be obtained otherwise by treating the quantization errors in the Gaussian process x(t) as independent and uniformly distributed between $-\Delta/2$ and $\Delta/2$.

The second is the clipping error which occurs when the input voltage is greater than the maximum quantizer level. The dynamic range of the input is seriously restricted in the presence of the quantizer, a form of limiter, which in turn regulates the clutter residue at the digital MTI output. Unfortunately, the quantizer causes the spectrum of the clutter to spread so that the MTI performance in the presence of limiting falls short of the performance predicted from linear theory. Ward and Shrader [17] computed the MTI improvement factor from the autocorrelation function for limited clutter (i.e., clutter after bandpass limiting). They chose a clutter model with a Gaussian autocorrelation function, and a limiter with an error function characteristic because a simple expression derived by Baum [18] relates the input and limited output autocorrelation functions when the input statistics are Gaussian. The results they found are verified by time-domain Monte Carlo simulation. They concluded that limiting must be included in any analysis of the MTI performance in order to achieve meaningful results. The presence of limiting may degrade the MTI

improvement factor by a large amount. For example, in the analysis of the double canceller MTI, a degradation as large as 20 dB may occur [17]. In the presence of another clutter model, in which the input statistic is neither Gaussian nor quasi-Gaussian, Grasso [19] has shown that limiting has the similar impact on the degradation of the MTI performance. He summarized that the improvement factor remains practically unchanged in the case of a single canceller MTI, but that the improvement factor of the double canceller is seriously reduced.

Tong [15] analyzed the performance of the MTI with uniform quantizers. In his paper, he computed the clutter attenuation of the MTI by making use of an expression derived by Velichkin [20] which utilizes the quantized normalized correlation coefficient. This expression takes into account the combined effects of both types of errors discussed above. Since we are going to rely heavily on this expression for obtaining the MTI clutter attenuation, we shall derive it here for completeness.

## 3.3 Output Correlation and Clutter Attenuation

Given a zero-mean Gaussian stationary random process x(t), it is level-quantized by a symmetrical quantizer with a step characteristic Q[x(t)] which is given by

$$Q[x(t)] = w_1 + \sum_{k=1}^{M-1} \int_{-\infty}^{x(t)} \Delta_k \delta(\eta - a_k)\, d\eta \qquad (3.9)$$

where $\delta(\eta - a_k)$ is the delta function, M is the total number of quantization levels of the step characteristic; $w_1$ is the first output level; $\Delta_k = w_{k+1} - w_k$ is the $k^{th}$ step size of the quantizer; $a_k$ is the $k^{th}$ threshold spacing of the quantizer. The typical quantizers are shown in Figs. 3.4 and 3.5.

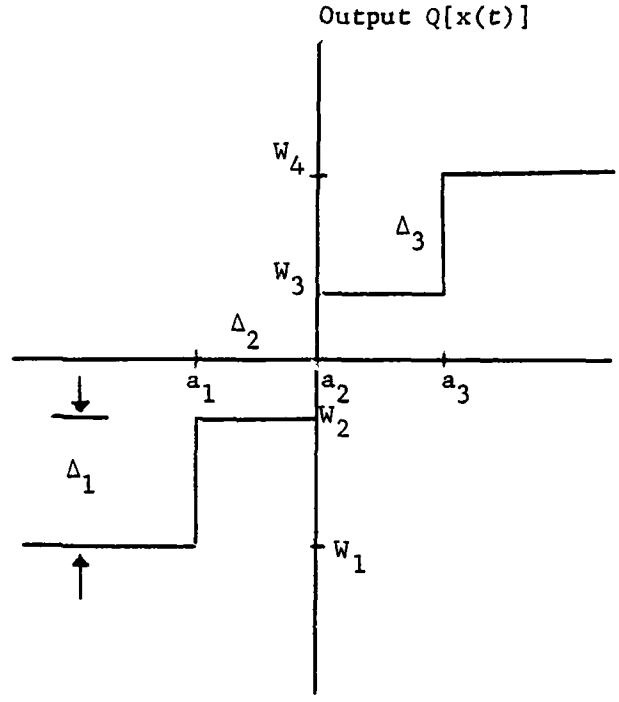


Figure 3.4. Quantizer with even number of levels (M = 4).

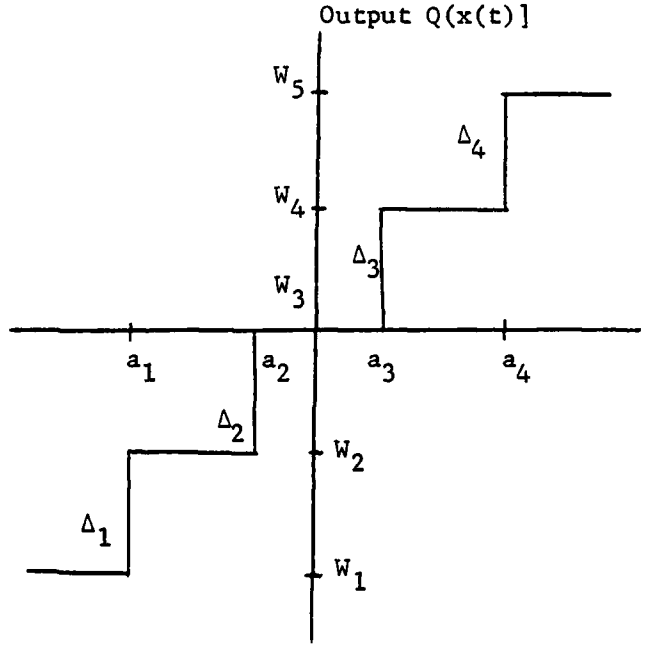


Figure 3.5. Quantizer with odd number of levels (M = 5).

The autocorrelation function, $R_Q(\tau)$, of the quantized Gaussian process is the joint moment of $Q[x(t+\tau)]$ and $Q[x(t)]$ and is defined as

$$R_Q(\tau) = E\{Q[x(t+\tau)]Q[x(t)]\} = \int_{-\infty}^{\infty}\int_{-\infty}^{\infty} Q(u)Q(v)f(u,v;\tau)dudv \qquad (3.10)$$

where $u = x(t+\tau)$; $v = x(t)$; $f(u,v;\tau)$ is the second order Gaussian probability density of the process $x(t)$.

The second order Gaussian probability density can be written in terms of the Hermite polynomials and the corresponding first order probability densities [21]

$$f(u,v,\tau) = f(u)f(v) \sum_{n=0}^{\infty} \frac{\rho_x^n(\tau)}{n!} H_n(\frac{u}{\sigma_x})H_n(\frac{v}{\sigma_x}) \qquad (3.11)$$

where $f(x)$ is the first order Gaussian probability density; $\rho_x(\tau)$ is the normalized correlation coefficient of $x(t)$; and $H_n(x)$ is the Hermite polynomials of degree n defined by [22]

$$H_n(x) = (-1)^n e^{x^2/2} \frac{d^n\{e^{-x^2/2}\}}{dx^n} = (-1)^n\sqrt{2\pi}\, e^{x^2/2}\, \Phi^{(n+1)}(x) \qquad (3.12)$$

where

$$\Phi(t) = \int_{-\infty}^{t} \frac{1}{\sqrt{2\pi}} e^{-x^2/2}dx \quad . \qquad (3.13)$$

Substituting (3.12) into (3.11), $f(u,v,\tau)$ becomes

$$f(u,v,\tau) = \frac{1}{\sigma_x^2} \sum_{n=0}^{\infty} \frac{\rho_x^n(\tau)}{n!} \Phi^{(n+1)}(\frac{u}{\sigma_x})\Phi^{(n+1)}(\frac{v}{\sigma_x}) \qquad (3.14)$$

Putting (3.14) into (3.10), $R_Q(z)$ is then written as

$$R_Q(\tau) = \frac{1}{\sigma_x^2} \sum_{n=0}^{\infty} \frac{\rho_x^n(\tau)}{n!} \left[ \int_{-\infty}^{\infty} Q(u) \Phi^{(n+1)}(\frac{u}{\sigma_x}) du \right]^2 \tag{3.15}$$

Since Q(u) is odd symmetric, and $\Phi^{(n)}(\frac{u}{\sigma_x})$ is even symmetric for n even, the sum of the terms, where n is even, equals to zero. With this mocification, Eq. (3.15) becomes

$$R_Q(\tau) = \frac{1}{\sigma_x^2} \sum_{\substack{n=1 \\ n \text{ odd}}}^{\infty} \frac{\rho_x^n(\tau)}{n!} \left[ \int_{-\infty}^{\infty} Q(u) \Phi^{(n+1)}(\frac{u}{\sigma_x}) du \right]^2 \tag{3.16}$$

Using the technique of integration by parts

$$\int_{-\infty}^{\infty} Q(u) \Phi^{(n+1)}(\frac{u}{\sigma_x}) du = - \sigma_x \int_{-\infty}^{\infty} Q^{(1)}(u) \Phi^{(n)}(\frac{u}{\sigma_x}) du \tag{3.17}$$

Differentiating (3.9) with respect to u, we get

$$Q^{(1)}(u) = \sum_{k=1}^{M-1} \Delta_k \delta(u - a_k) \tag{3.18}$$

Substituting (3.18) into (3.17), we obtain

$$\int_{-\infty}^{\infty} Q(u) \Phi^{(n+1)}(\frac{u}{\sigma_x}) du = - \sigma_x \sum_{k=1}^{M-1} \Delta_k \Phi^{(n)}(\frac{a_k}{\sigma_x}) \tag{3.19}$$

With the help of Eq. (3.19), $R_Q(\tau)$ has the form

$$R_Q(\tau) = \sum_{\substack{n=1 \\ n \text{ odd}}}^{\infty} \left[ \sum_{k=1}^{M-1} \Delta_k \Phi^{(n)}(\frac{a_k}{\sigma_x}) \right]^2 \frac{\rho_x^n(\tau)}{n!} \tag{3.20}$$

Since $\Phi^{(n)}(x)$ is related to $H_{n-1}(x)$ by Eq. (3.12), Eq. (3.20) becomes

$$R_Q(\tau) = \sum_{\substack{n=1 \\ n \text{ odd}}}^{\infty} \left[ \sum_{k=1}^{M-1} \Delta_k \exp(-a_k^2/2\sigma_x^2) H_{n-1}(a_k/\sigma_x) \right]^2 \frac{\rho_x^n(\tau)}{2\pi n!} \tag{3.21}$$

The variance, $\sigma_Q^2$, of the quantization process is determined by equating $\tau$ to zero in Eq. (3.21). Then

$$\sigma_Q^2 = R_Q(0) = \sum_{\substack{n=1 \\ n \text{ odd}}}^{\infty} \left[ \sum_{k=1}^{M-1} \Delta_k \exp(-a_k^2/2\sigma_x^2) H_{n-1}(a_k/\sigma_x) \right]^2 \Big/ 2\pi n! \tag{3.22}$$

The normalized correlation coefficient, $\rho_Q(\tau)$ of the quantized process is thus

$$\rho_Q(\tau) = \frac{R_Q(\tau)}{R_Q(0)} = \frac{R_Q(\tau)}{\sigma_Q^2} = \frac{1}{2\pi\sigma_Q^2} \sum_{\substack{n=1 \\ n \text{ odd}}}^{\infty} \left[ \sum_{k=1}^{M-1} \Delta_k \exp(-a_k^2/2\sigma_x^2) H_{n-1}(a_k/\sigma_x) \right]^2 \cdot \frac{\rho_x^n(\tau)}{n!} \tag{3.23}$$

Since $\rho_Q(\tau)$ and $\sigma_Q^2$ are infinite series, they can only be evaluated numerically. A stopping rule for the evaluations of them is provided in Tong's paper [15].

The clutter attenuation, a performance criterion of an MTI system, relates the input power and the output power of the MTI. Mathematically, for the Gaussian clutter model in which the input clutter x(t) is a zero mean stationary Gaussian random process, the input power is $\sigma_x^2 = E\{x^2(t)\}$. The output power $\sigma_y^2$, of a single canceller MTI is

$$\sigma_y^2 = E\{y^2(t)\} = E\{[x(t)-x(t+D)]^2\} = 2\sigma_x^2[1-\rho_x(D)] \tag{3.24}$$

and the output power of a double canceller MTI is

$$\sigma_y^2 = E\{[x(t)-2x(t+D)+x(t+2D)]^2\} = 6\sigma_x^2[1-\frac{4}{3}\rho_x(D)+\frac{1}{3}\rho_x(2D)] \tag{3.25}$$

The clutter attenuation, CA, for these MTI's are

$$CA^{(1)} = \frac{\sigma_x^2}{\sigma_y^2} = \frac{1}{2[1-\rho_x(D)]} \tag{3.26}$$

$$CA^{(2)} = \frac{1}{6[1-\frac{4}{3}\rho_x(D)+\frac{1}{3}\rho_x(2D)]} \tag{3.27}$$

respectively. Similarly, the CAs for the quantized MTI system are

$$CA_Q^{(1)} = \frac{1}{2[1-\rho_Q(D)]} \tag{3.28}$$

$$CA_Q^{(2)} = \frac{1}{6[1-\frac{4}{3}\rho_Q(D)+\frac{1}{3}\rho_Q(2D)]} \tag{3.29}$$

Notice that for the double canceller MTI, $CA^{(2)}$ is a function of $\rho_x(D)$ and $\rho_x(2D)$. However, $\rho_x(D)$ and $\rho_x(2D)$ are directly related to one another for the Gaussian assumption. Recall the correlation function for the Gaussian clutter model is given by Eq. (2.4) and is repeated here

$$\rho_x(\tau) = \exp(-\tau^2/2\sigma_\tau^2). \tag{3.30}$$

Similarly $\rho_x(2D)$ can be shown as

$$\rho_x(2D) = \exp(-(2D)^2/2\sigma_\tau^2) = [\exp(-D^2/2\sigma_\tau^2)]^4 = \rho_x^4(D). \tag{3.31}$$

Hence, the clutter attenuation for both linear MTIs are described solely by the linear correlation coefficient, $\rho_x(D)$, while the clutter attenuation for both quantized MTIs are governed by the two corresponding quantized correlation coefficients $\rho_Q(D)$ and $\rho_Q(2D)$, which are both in terms of the step size $\Delta_k$, the threshold spacing $a_k$, the variance of the input process $\sigma_x^2$, the total number of the quantization levels M, and the linear correlation coefficient $\rho_x(D)$.

In order to compare the performance of the linear MTI and the quantized MTI, the loss factor, $\gamma$, is defined as the loss introduced due to quantization, in which for the single and double canceller MTIs are

$$\gamma = \frac{CA^{(1)}}{CA_Q^{(1)}} \tag{3.32}$$

and

$$\gamma = \frac{CA^{(2)}}{CA_Q^{(2)}} \tag{3.33}$$

respectively.

In the following sections of this thesis Eqs. (3.23), (3.31), (3.32), and (3.33) will be used extensively for analyzing the performance of the single and double canceller MTIs with uniform quantizers, logarithmic quantizers and $\mu$-law quantizers respectively.

## 3.4 Uniform Quantization in Digital MTI

With the above tools, Tong [15] has analyzed the performance of the single and double canceller MTIs with uniform quantizer as a function of the number of quantizer levels and the spacing of these levels. His analysis considers only the even quantizer, i.e., M is even. A uniform

quantizer, as its name implies, has a uniform threshold spacing and uniform step size. Without loss of generality, unit step size is assumed. For simplicity, a normalized spacing between thresholds of an M-level uniform quantizer is denoted as $\alpha = a_k/\sigma_x$. The uniform threshold spacings of the uniform quantizer are then located at $k\alpha$ where $k$ is an integer which goes from -(M/2-1) to (M/2-1) including k = 0. With the above modifications, $\rho_Q(\tau)$, for the uniform quantizer, can be shown to be

$$\rho_Q(\tau) = \frac{2}{\pi\sigma_Q^2} \sum_{\substack{n=1 \\ n \text{ odd}}}^{\infty} \left[ \sum_{k=0}^{M/2-1} \Delta_k \exp(-(k\alpha)^2/2) H_{n-1}(k\alpha) \right]^2 \frac{\rho_x^n(\tau)}{n!} \qquad (3.34)$$

where $\Delta_k = \frac{1}{2}$ for k = 0, and $\Delta_k = 1$ for $k \neq 0$.

In order to test our computer program, we verified Tong's results by using Eq. (3.34) for uniform quantizer with even numbers of levels. Examples of the results are given in Figs. 3.6-3.9 which depict the loss of the single and double canceller MTIs with 8 and 32 level uniform quantizers. On the basis of similar results, Tong concluded that the best uniform quantizer threshold spacing is a function of the input clutter power and the clutter correlation property. The best $\alpha$ is found to be strongly dependent on the value of $\rho_x$, especially in the case when the number of quantizer levels is small (see figs. 3.6 and 3.8). There is always an optimum $\alpha$ for each input correlation function $\rho_x(D)$. A nonoptimum spacing can result in a loss significantly greater than the minimum. Therefore, if clutter input is expected to change widely,

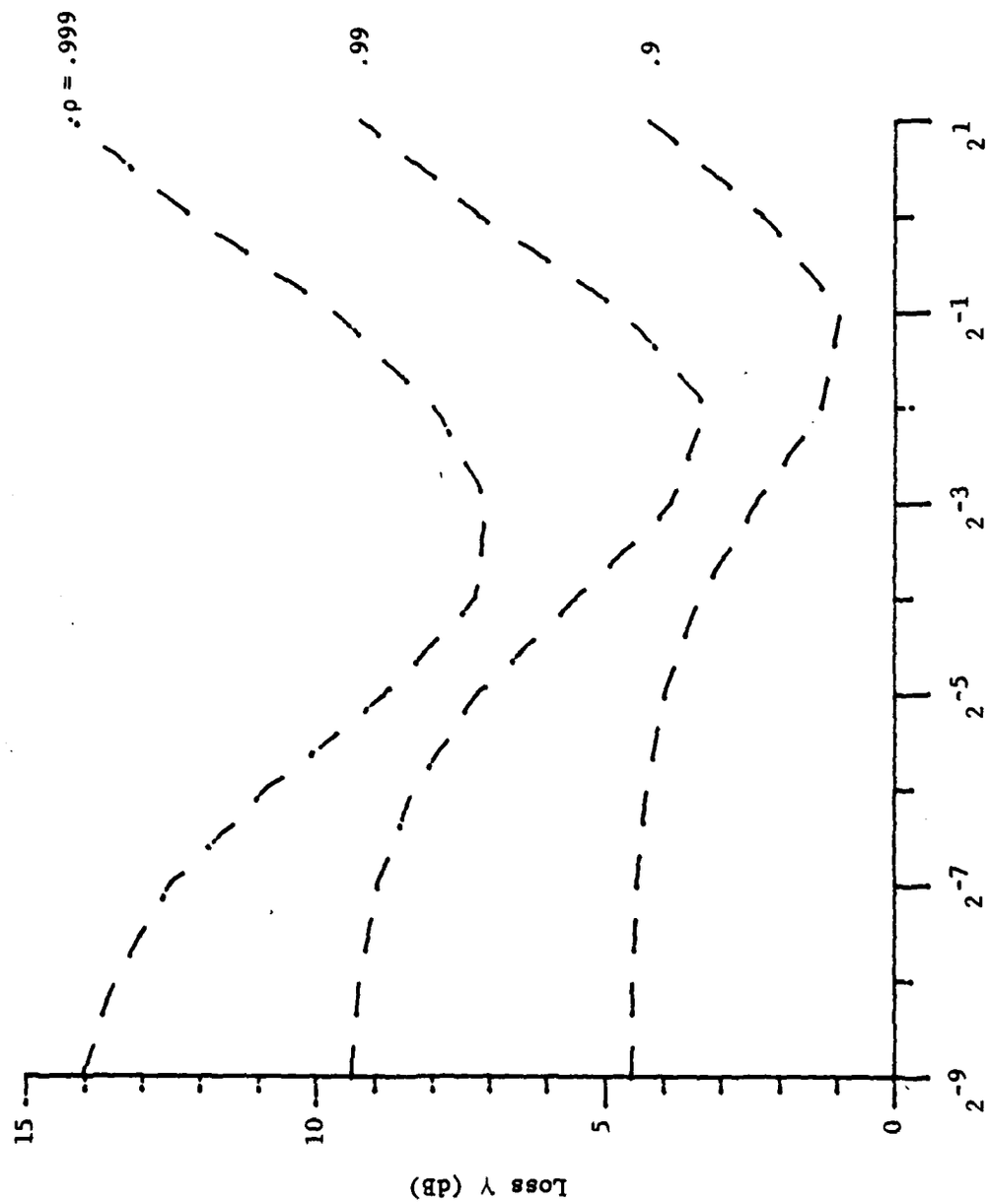


Figure 3.6. Loss of single canceller MTI with 8-level uniform quantizer.

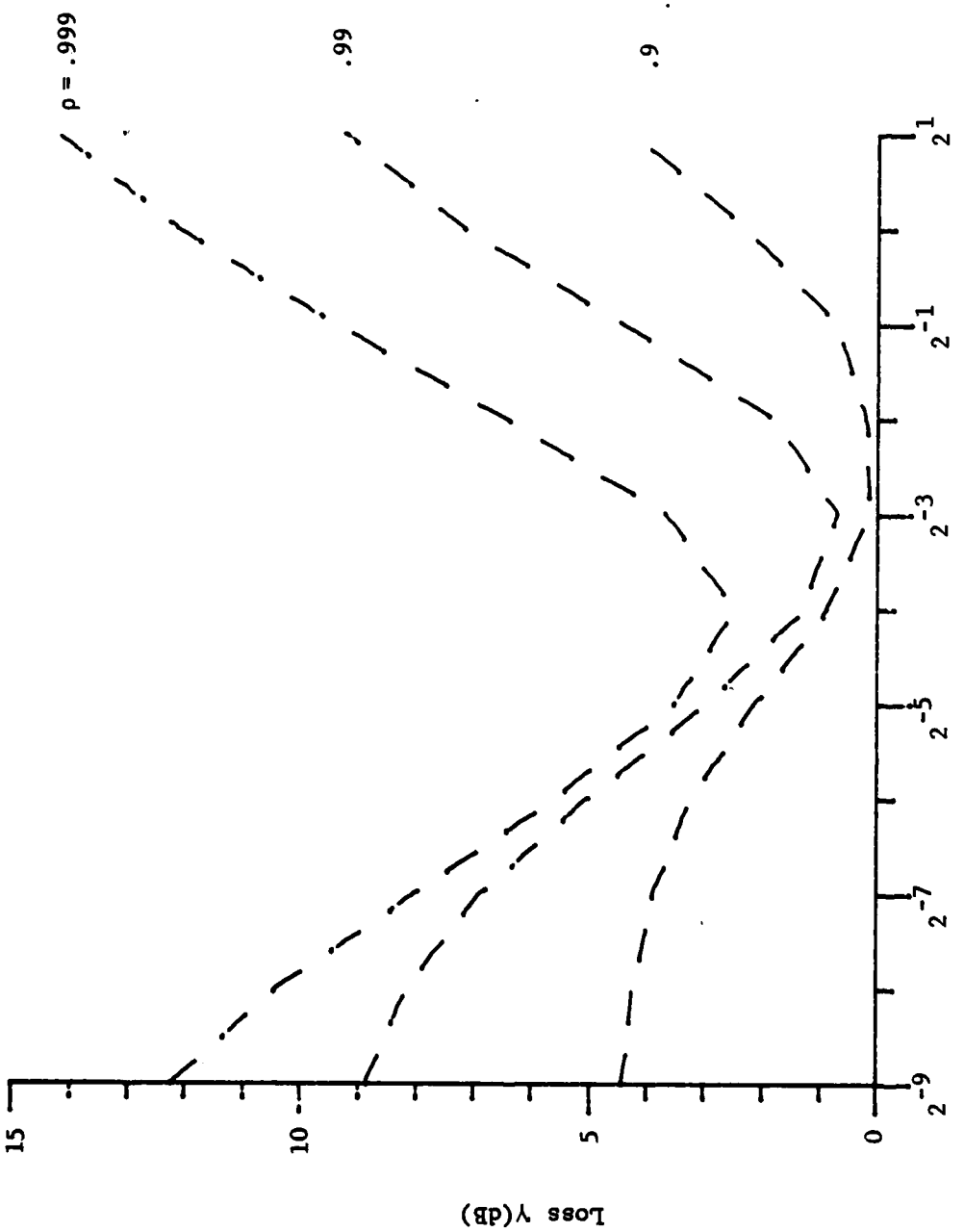


Figure 3.7. Loss of single canceller MTI with 32-level uniform quantizer.

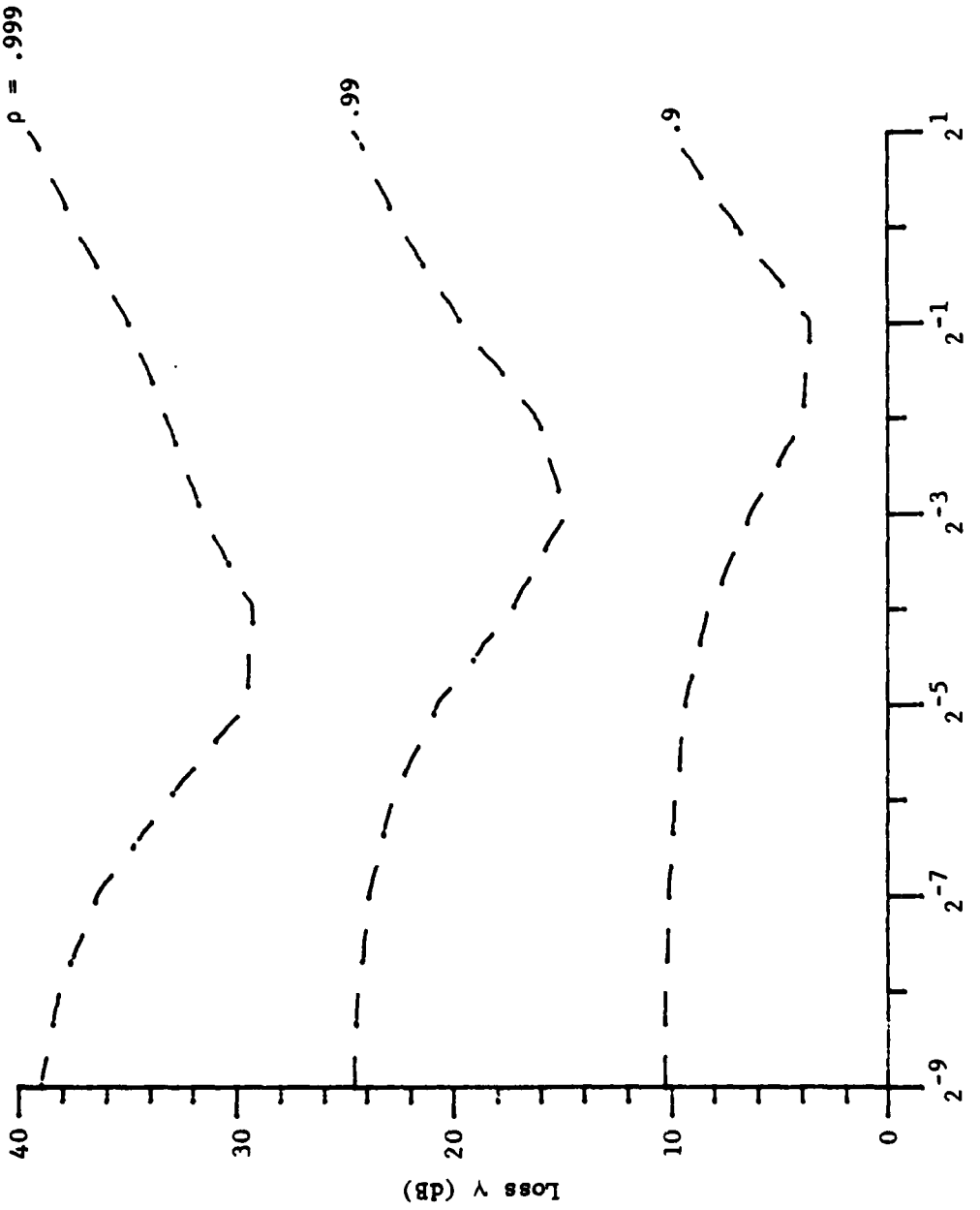


Figure 3.8. Loss of double canceller MTI with 8 level uniform quantizer.

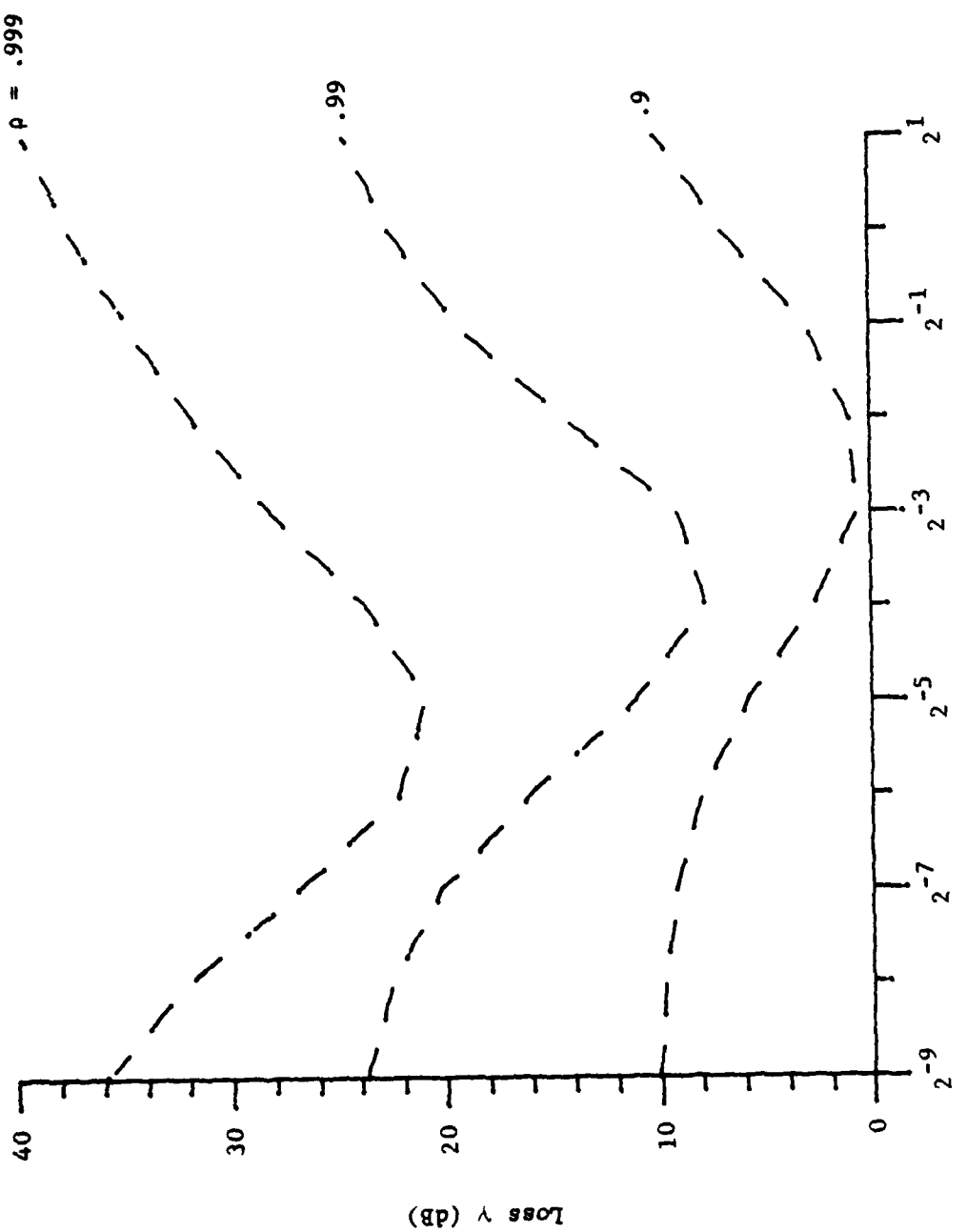


Figure 3.9. Loss of double canceller MTI with 32-level uniform quantizer.

optimum threshold is desirable to adapt to local clutter conditions. Furthermore, as the number of output levels is increased, the minimum loss is reduced considerably and the optimum $\alpha$ setting is less critically dependent on the input correlation coefficient. However, if the threshold spacing is either too small or too big, as Tong noted, the quantizer acts as a hard limiter and the loss is maximum. $\rho_Q$, in this situation, is a function of $\rho$ and is given by [23]

$$\rho_Q = \frac{2}{\pi} \sin^{-1} \rho_x \tag{3.35}$$

For instance, when $\rho_x$ is 0.999, $\rho_Q$ approaches 0.9715, and $\gamma$ approaches 14.5 dB and 39.8 dB for the single and double canceller MTIs respectively.

By using techniques similar to those of Tong, the performance of the MTI with logarithmic and $\mu$-law quantizers will be discussed in the following section.

## 4. DIGITAL MTI PERFORMANCE FOR μ-LAW AND LOGARITHMIC QUANTIZERS

In this section, the effect of logarithmic and μ-law quantization on the performance of the single and double canceller MTI will be analyzed. Only odd-symmetric quantizers with number of output levels equal integral powers of 2 will be considered. Without loss of generality, unity step size and unit variance of input clutter process are assumed.

### 4.1. Logarithmic Quantizers

A logarithmic quantizer is modeled as a base-2 logarithmic nonlinearity, followed by a uniform quantizer. In this way, an M-level quantizer has the threshold spacings distributed at $a_k = \alpha 2^k$ for k representing integers between - (M/2-1) and (M/2-1). In this case, $\alpha$ is denoted as the threshold spacing for the logarithmic quantizer. Note that this definition is different from the one defined by Tong [15] for the uniform quantizer. For the computation of $\rho_Q(\tau)$ in this case, $k\alpha$ in Eq. (3.34) is replaced by $\alpha 2^k$. Hence $\rho_Q(2)$ for the logarihmic quantizer is given by

$$\rho_Q(2) = \frac{2}{\pi\sigma_Q^2} \sum_{\substack{n=1 \\ n \text{ odd}}} \left[ \sum_{k=0}^{M/2-1} \Delta_k \exp\{-\frac{(2^k\alpha)^2}{2}\} H_{n-1}(2^k\alpha) \right]^2 \frac{\rho_x^n(2)}{n!} \qquad (4.1)$$

where again $\Delta_k = \frac{1}{2}$ for $k = 0$, $\Delta_k = 1$ for $k \neq 0$.

### 4.2. Analysis of the MTI Performance with Logarithmic Quantizers

#### i) Single Canceller MTI

Apply $\rho_Q(2)$ of Eq. (4.1) to $\gamma$ of Eq. (3.32), the loss, incorporated with a 16 level quantizer, as a function of $\rho_x$ for different values of $\alpha$ is plotted in Fig. 4.1. The values of $\rho_x$ shown are ranging from 0.1 to 0.999. As $\rho_x$ approaches unity, the loss is infinite. This is the case

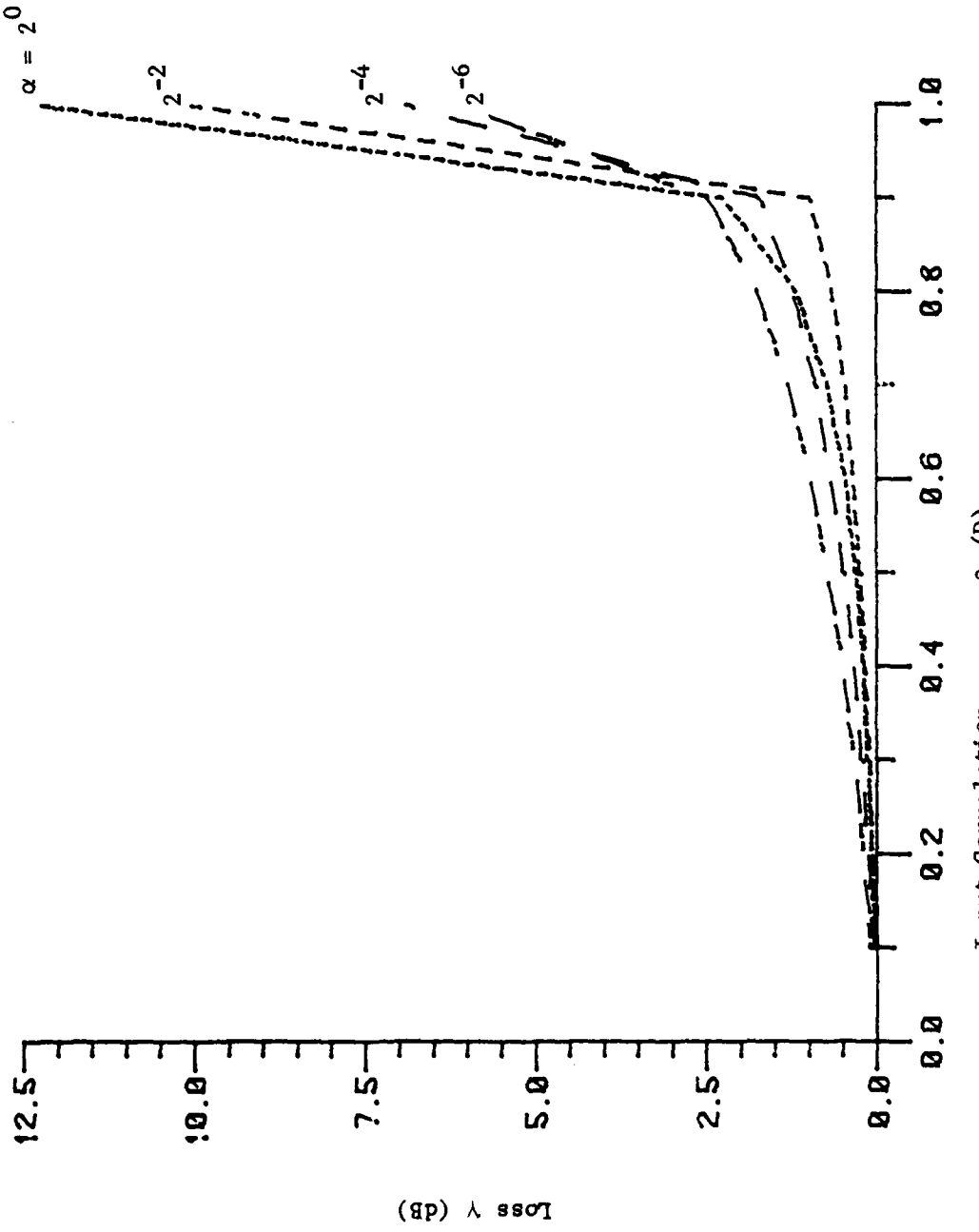


Figure 4.1. Loss of single canceller MTI with 16-level logarithmic quantizer.

when $x(t) = x(t+D)$ for perfectly correlated input clutter , corresponding to a zero MTI output. It is seen that, for this case, as the input clutter becomes more highly correlated, the loss rises significantly. The quantizer input correlation function $\rho_Q(\tau)$ is thus smaller than the linear input correlation function $\rho_x(\tau)$. However, all these are justified by the fact that the quantizer tends to decorrelate the clutter input because of the spread out of the clutter spectra in the presence of a quantizer. Hence the effectiveness of an MTI is reduced drastically. In case of lowly correlated input clutter, for instance $\rho_x < .9$, if the threshold spacing is not too big or too small, the performance of the digital MTI and linear MTI are almost the same regarding the degradation in performance. As shown in Fig. 4.1., the degradation is less than 2.5 dB for $\rho_x < .9$. As a result, we will be concentrating more on the performance of an MTI for highly correlated input clutter, in the sense that $\rho_x \geq 0.9$. It can be seen that the choice of $\alpha$ has a dramatic impact on the resulting loss of the digital MTI. Too large or too small a choice of $\alpha$ (i.e. $\alpha \to \infty$ or $\alpha \to 0$) will give rise to a maximum loss of 4.58, 9.55 and 14.54 in dB for input correlated coefficient $\rho_x = .9$, .99 and .999 respectively. Consider the 8 and 32 level logarithmic quantizers. The loss as a function of $\alpha$ is plotted in Figs. 4.2 and 4.3. For any value of M, it is found that there is always an optimum spacing for each input correlation. Nevertheless, at the setting of optimum spacing for both quantizers taken for $\rho_x = .999$, the minimum loss are 7.03 and 5.97 in dB for the 8 and 32 level quantizers respectively. Hence, the difference is only 1.06 dB in terms of improvement. With more quantizer levels, the loss can be diminished by a large amount. For instance, when $\rho_x = .999$, an improvement of 5 dB is achieved for a

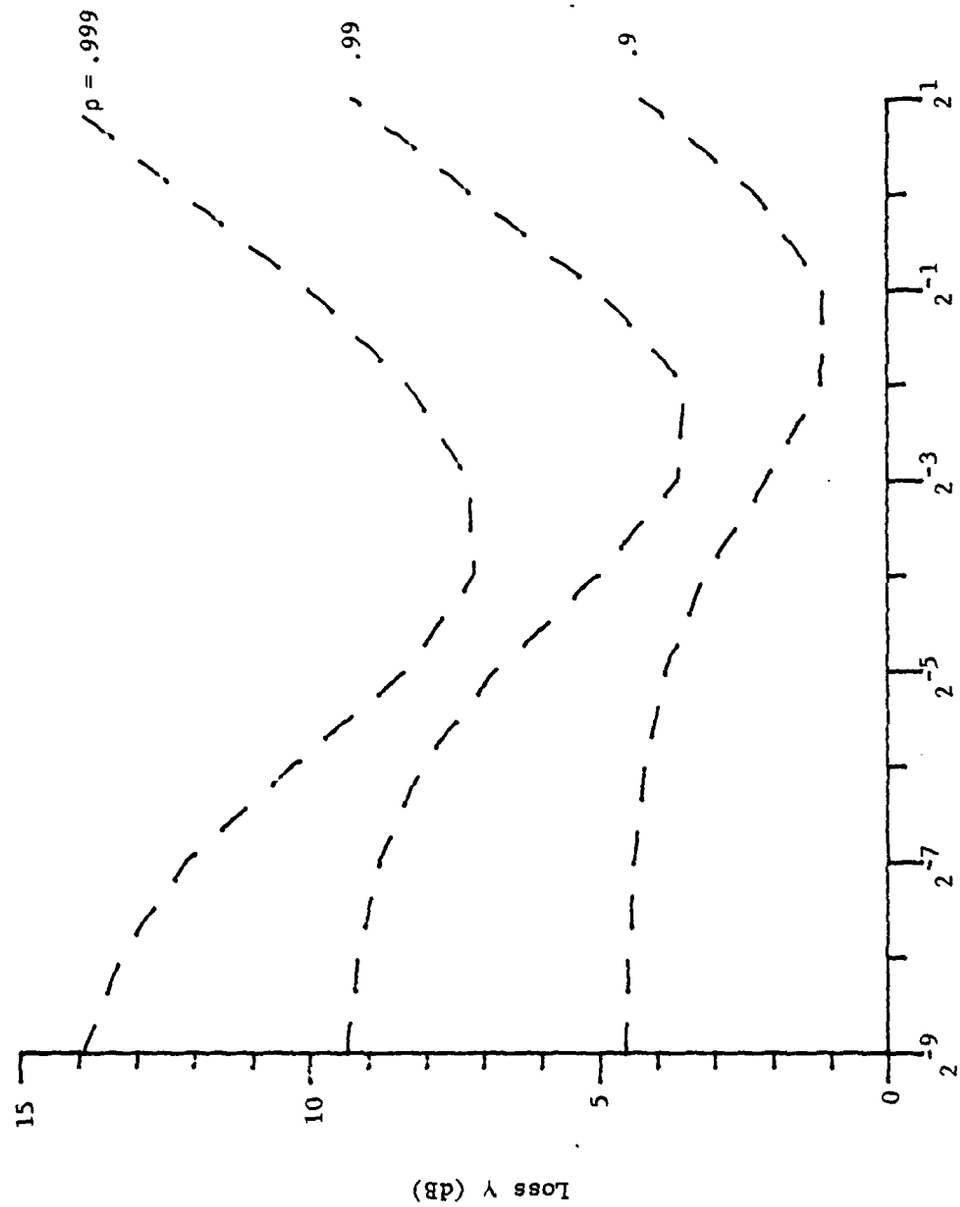


Figure 4.2. Loss of single canceller MTI with 8-level logarithmic quantizer.

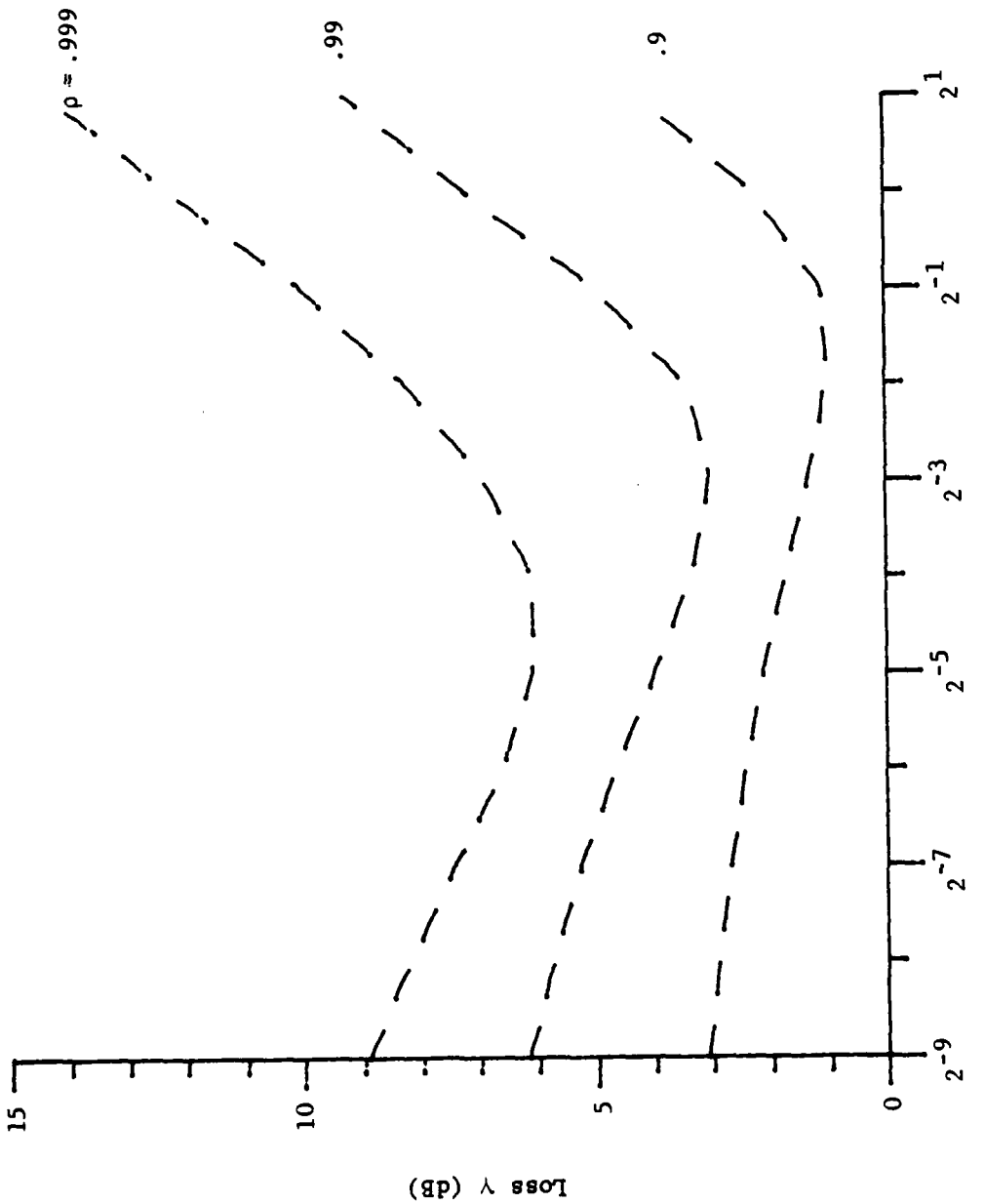


Figure 4.3. Loss of single canceller MTI with 32-level logarithmic quantizer.

32-level quantizer as compared to a 8-level quantizer, even though the spacing $\alpha = 2^{-9}$ is nonoptimum. Table 4.1 shows the minimum loss and optimum spacing with different number of output levels for $\rho_x = .9$, .99 and .999. It is found that a 16-level quantizer is almost as good as a 32-level quantizer at optimum setting of threshold spacing. Although the optimum spacing for M = 32 and 64 are the same, it can be shown that they vary a great deal at setting of nonoptimum spacing.

ii) Double Canceller MTI

Again the loss as a function of $\rho_x$ is plotted in Fig. 4.4. Here the loss is much greater than the loss of a single canceller. Theoretically, there is a progressive translation of power toward higher frequencies, and therefore the high filtering effect of the cancellation circuits is accentuated. This explains why the loss for the double canceller is so much higher than that for the single canceller. The loss for 8- and 32-level logarithmic quantizers is obtained and plotted in Figs. 4.5 and 4.6. The result shows that for spacing less than optimum spacing, the loss will be differentiated by a wide margin for M = 8 and 32; while for spacing greater than the optimum spacing, the loss is within 1 dB. Nevertheless, in the limit when the quantizer spacing becomes too large or too small, the loss can reach 10.32, 24.83 and 39.78 in dB for $\rho_x = .9$, .99 and .999 respectively. Table 4.2 shows the minimum loss and optimum $\alpha$ for different number of output levels.

## 4.3. $\mu$-Law Quantizers

A $\mu$-law quantizer is represented by a memoryless nonlinearity function $g(x) = V \log(1+\mu x/V)/\log(1+\mu)$ (where $\mu > 0$ and $V > 0$), followed by a uniform quantizer. The nonlinearity is defined as a $\mu$-law, or logarithmic

Table 4.1. Single canceller MTI with logarithm quantizer for optimum and minimum loss.

| $\rho_x$ | .9 | | .99 | | .999 | |
|---|---|---|---|---|---|---|
| Number of Levels | Optimum $\alpha$ | Minimum Loss (dB) | Optimum $\alpha$ | Minimum Loss (dB) | Optimum $\alpha$ | Minimum Loss (dB) |
| 4 | .609 | 2.14216963 | .268 | 5.73887474 | .105 | 10.1381723 dB |
| 8 | .358 | .9884949 | .185 | 3.35583555 | .085 | 7.02795208 |
| 16 | .387 | .96757299 | .126 | 3.01448506 | .045 | 5.9733119 |
| 32 | .386 | .96757273 | .126 | 3.01448506 | .045 | 5.97327101 |

Table 4.2. Double canceller with logarithm quantizer for optimum loss and minimum loss.

| $\rho_x$ | .9 | | .99 | | .999 | |
|---|---|---|---|---|---|---|
| Number of Levels | Optimum $\alpha$ | Minimum Loss (dB) | Optimum $\alpha$ | Minimum loss (dB) | Optimum $\alpha$ | Minimum loss (dB) |
| 4 | .538 | 6.17393225 | .188 | 19.1853588 | .062 | 33.697058 |
| 8 | .311 | 3.51007134 | .108 | 14.9583513 | .036 | 29.1079888 |
| 16 | .281 | 3.45113233 | .079 | 14.7207975 | .023 | 28.471298 |
| 32 | .281 | 2.54112962 | .079 | 14.7207975 | .023 | 28.4720766 |

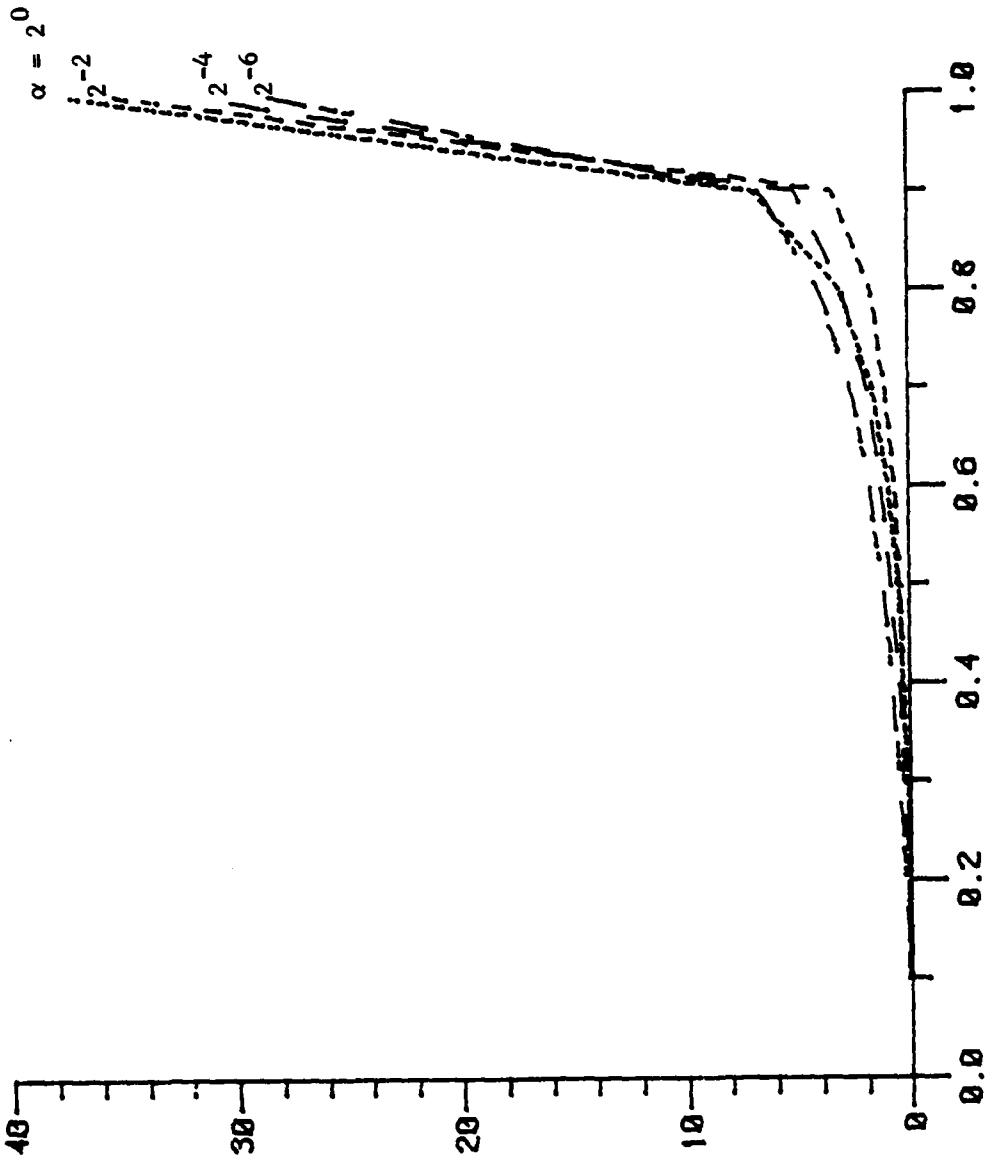


Figure 4.4. Loss of double canceller MTI with 16-level logarithmic quantizer.

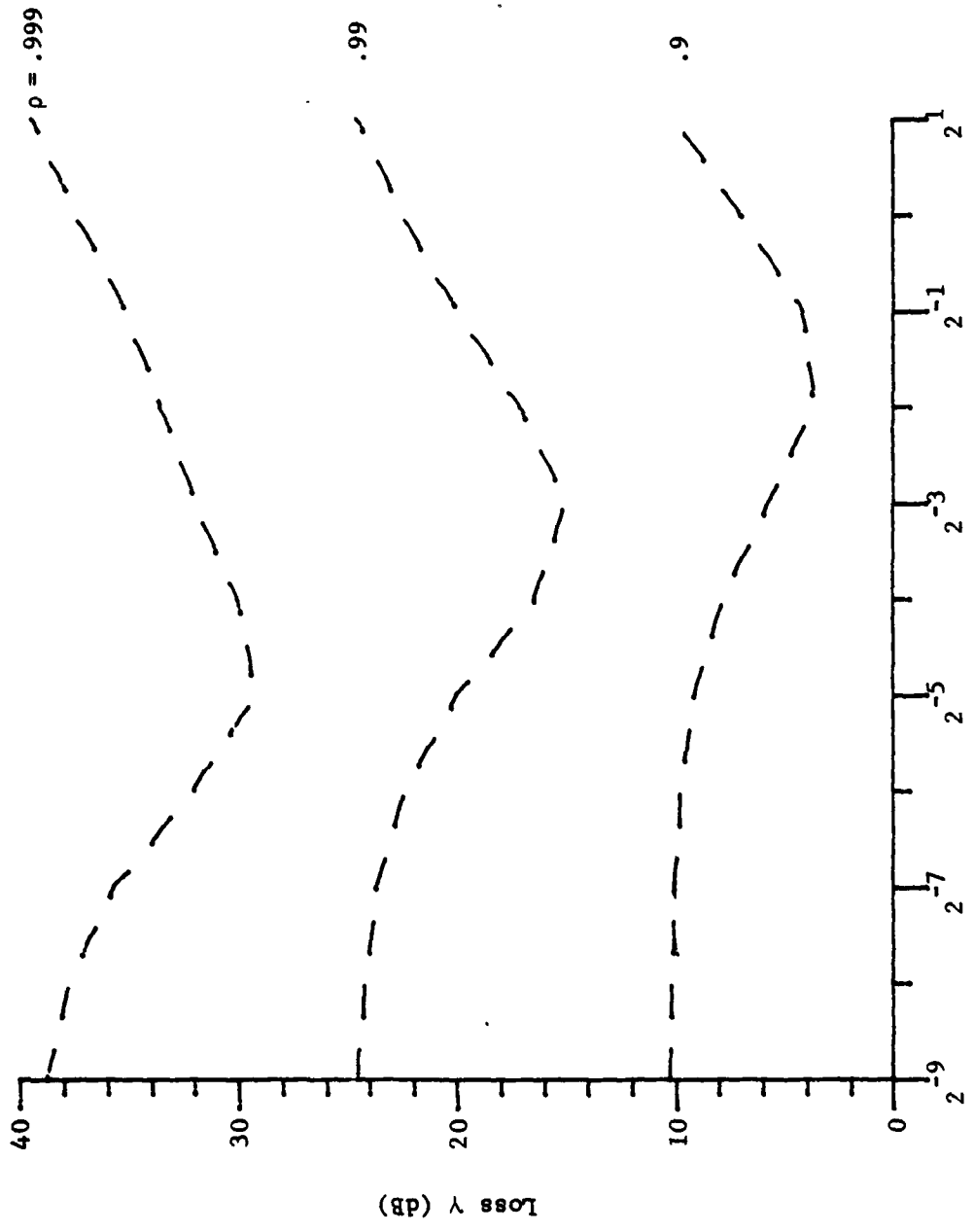


Figure 4.5. Loss of double canceller MTI with 8-level logarithmic quantizer.

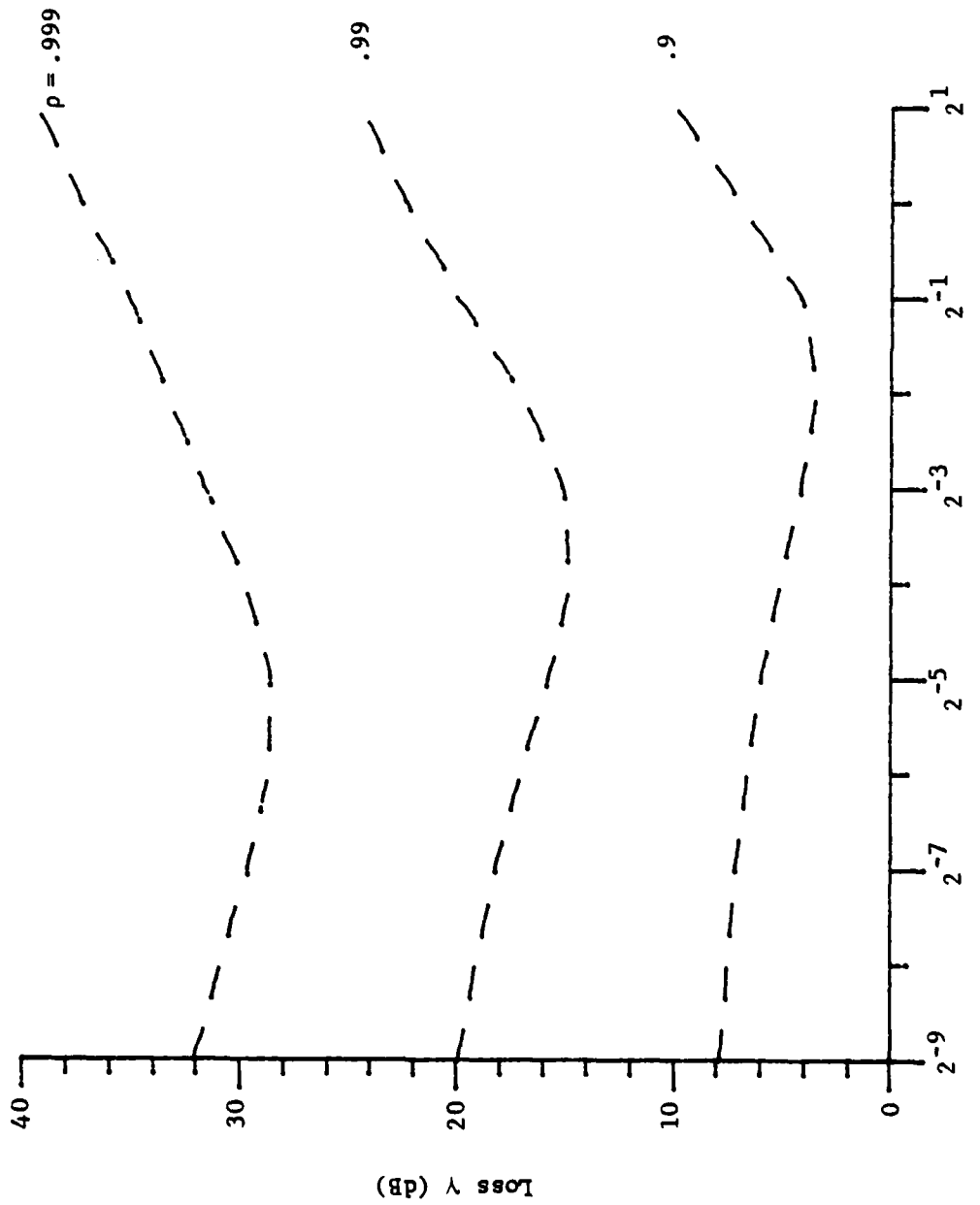


Figure 4.6. Loss of double canceller MTI with 32-level logarithmic quantizer.

compression, curve [24] where $\mu$ is a compression parameter which controls the degree of compression and may be chosen so that large changes in the input produce relatively small charge in the output; and V is the preset maximum input voltage. The nonlinearity spreads out low amplitude input clutter over a large range while shrinking the higher amplitude input clutter into a smaller region. The effect is to allocate more quantization levels to the lower amplitudes, which generally have higher probability. In this case, the spacing of the quantizer levels, which is a function of $\mu$ and V, is located at $a_k = \frac{V}{\mu}\,[(1+\mu)^{k/V}-1]$ instead of $\alpha 2^k$ as for the logarithmic quantizer. Apply $a_k$ to Eq. (3.34), $\rho_Q(\tau)$ for the $\mu$-law quantizer is given by

$$\rho_Q(\tau) = \frac{2}{\pi\sigma_Q^2} \sum_{n=1}^{\infty} \left[ \sum_{k=0}^{M/2-1} \Delta_k \exp\{-[\tfrac{V}{\mu}[(1+\mu)^{k/V}-1]]^2/2\} H_{n-1}\{\tfrac{V}{\mu}[(1+\mu)^{k/V}-1]\} \right]^2 \cdot \frac{\rho_x^{\,n}(\tau)}{n!} \tag{4.2}$$

where $\Delta_k = \frac{1}{2}$ for $k = 0$, $\Delta_k = 1$ for $k \neq 0$.

4.4. Analysis of the MTI Performance with $\mu$-Law Quantizers.

i) Single Canceller MTI

With $\mu = 1$, 10 and 100, V = 100, the loss is plotted with respect to $\rho_x$ from .1 to .999 for a 16-level quantizer and is shown in Fig. 4.7. As analogous to the logarithmic quantizer, the loss of the digital MTI increases significantly as the input clutter becomes highly correlated, i.e. for $\rho_x \geq .9$. The quantizer experiences the biggest loss when a compression parameter of 100, the largest of the three, is chosen for $\rho_x \leq .9$. When $\mu$ is large, the output levels are crowded about zero.

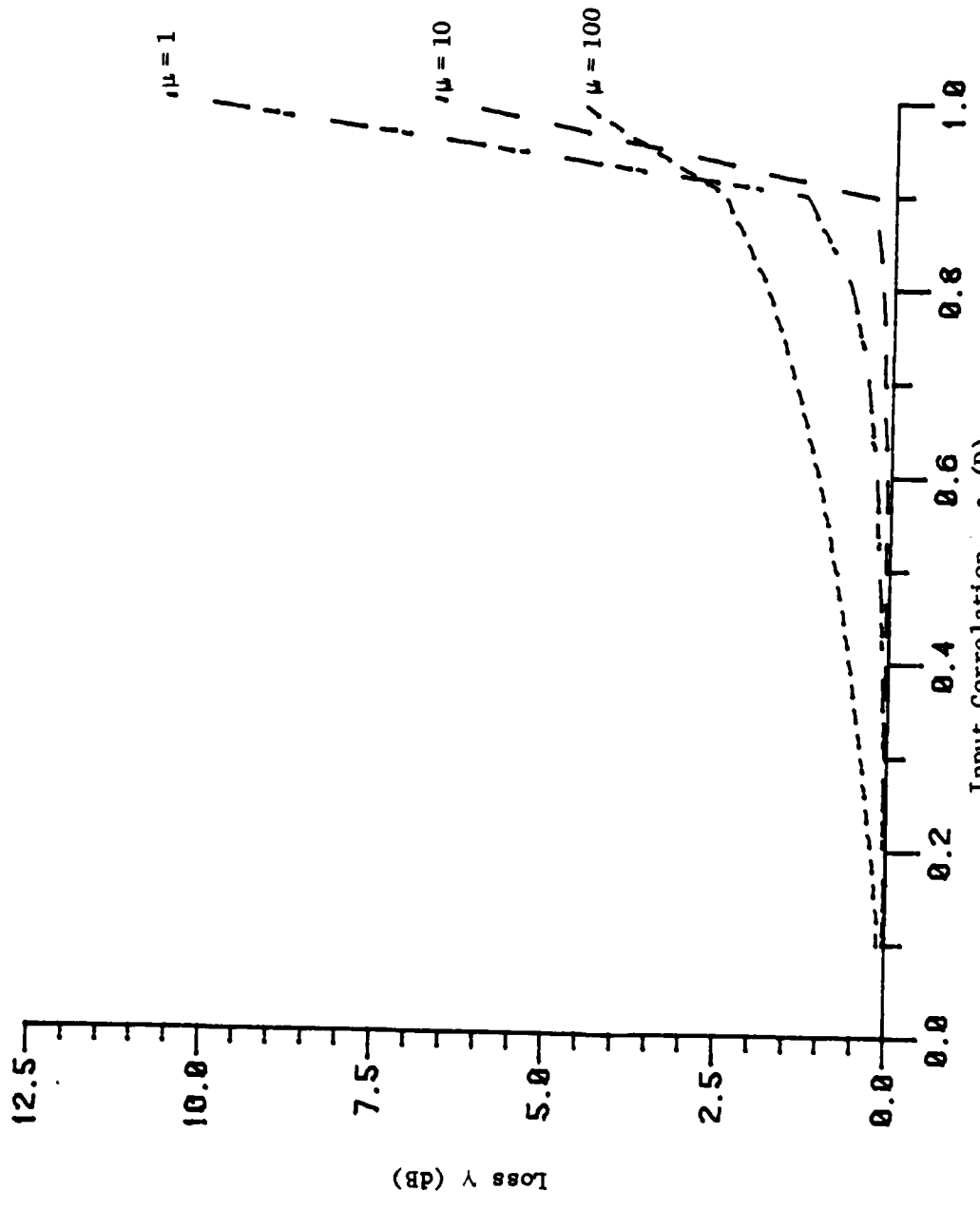


Figure 4.7. Loss of single canceller MTI with 16-level μ-law quantizer and V = 100.

In the limit when $\mu$ approaches $+\infty$, the quantizer behaves essentially as a hard limiter, the maximum loss is exactly the same as that obtained for the uniform and logarithmic quantizers. For highly correlated input clutter, $\mu = 100$ comes out to be the best of the three. Figure 4.7 does indicate that the choice of $\mu$ is vital to the performance of digital MTI. Again, the following discussion will be restricted to highly correlated input clutter with $\rho_x \geq 0.9$. Results of 8 and 32 level quantizers with $V = 10$ are shown in Fig. 4.8 and Fig. 4.9. Intutively, for any given M, there is an optimum $\mu$ which gives rise to a minimum loss. Indeed, the optimum $\mu$ occurs for each $\rho_x$. However, it is interesting to find that the optimum $\mu$ tends to increase as the input correlation function $\rho_x$ increases. As optimum $\mu$'s of $M = 8$ are compared to those of $M = 32$, it can be seen that with more quantizer levels, the optimum compression parameter is incremented by a great deal. For instance at $\rho_x = .999$, the compression parameters at minimum loss are 79 and 165 for $M = 8$ and 32 respectively. With V set at 1000, the loss of 8 and 32 level quantizers are plotted in Figs. 4.10 and 4.11. The results here are analogous to the $V = 10$ case. Again each of the loss curves shows an optimum $\mu$ coupling to a minimum loss. A close examination of Figs. 4.8-4.11 reveal some interesting results. Each of the optimum $\mu$'s and their corresponding loss at $V = 1000$ is smaller than that obtained at $V = 10$. It implies that an improvement in the performance can be achieved by a combined action: increasing the number of quantizer levels and allowing a large preset input voltage. Table 4.3 lists the optimum $\mu$'s and their corresponding loss with $V = 10$ for various output levels.

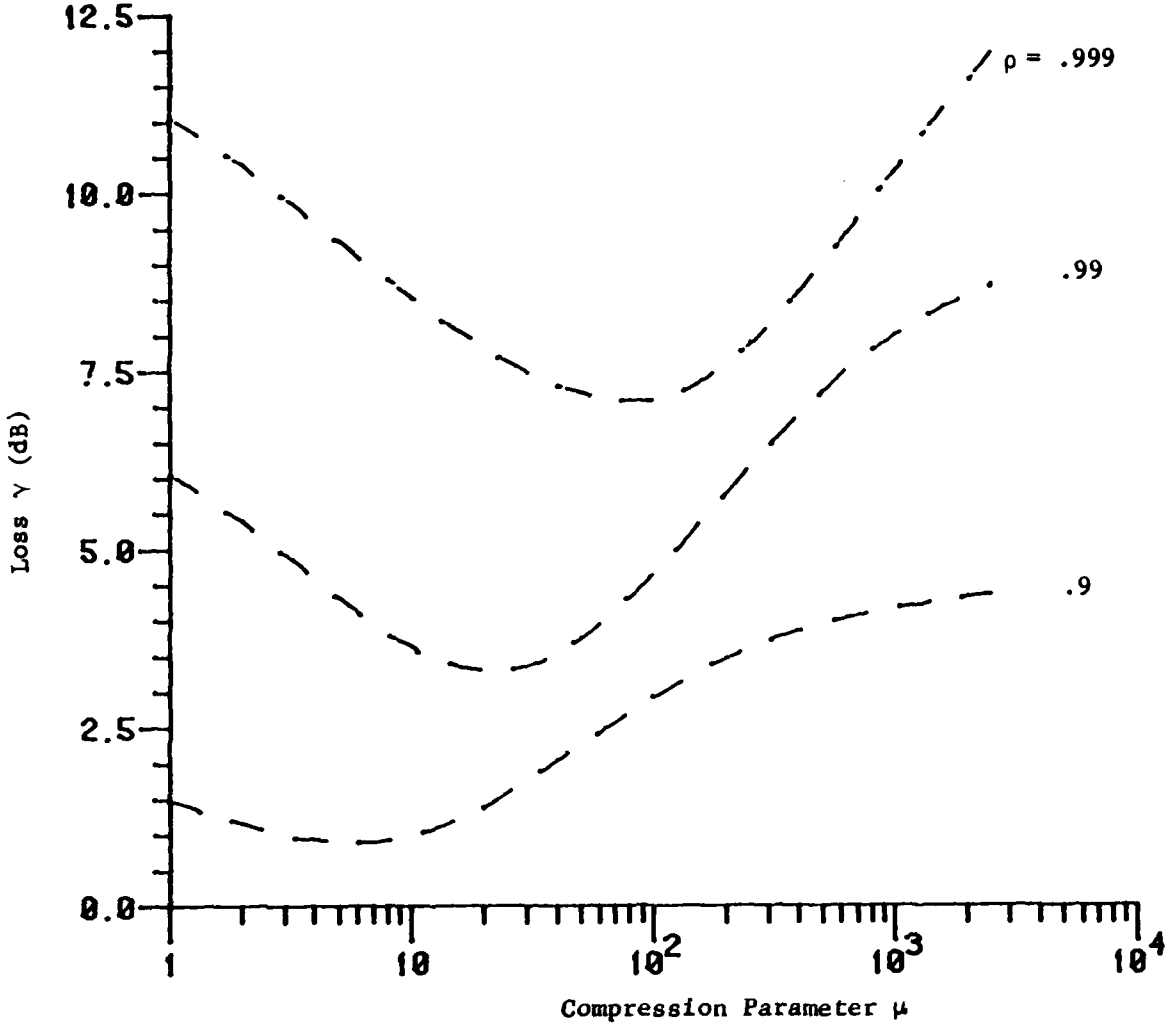


Figure 4.8. Loss of single canceller MTI with 8-level μ-law quantizer and V = 10.

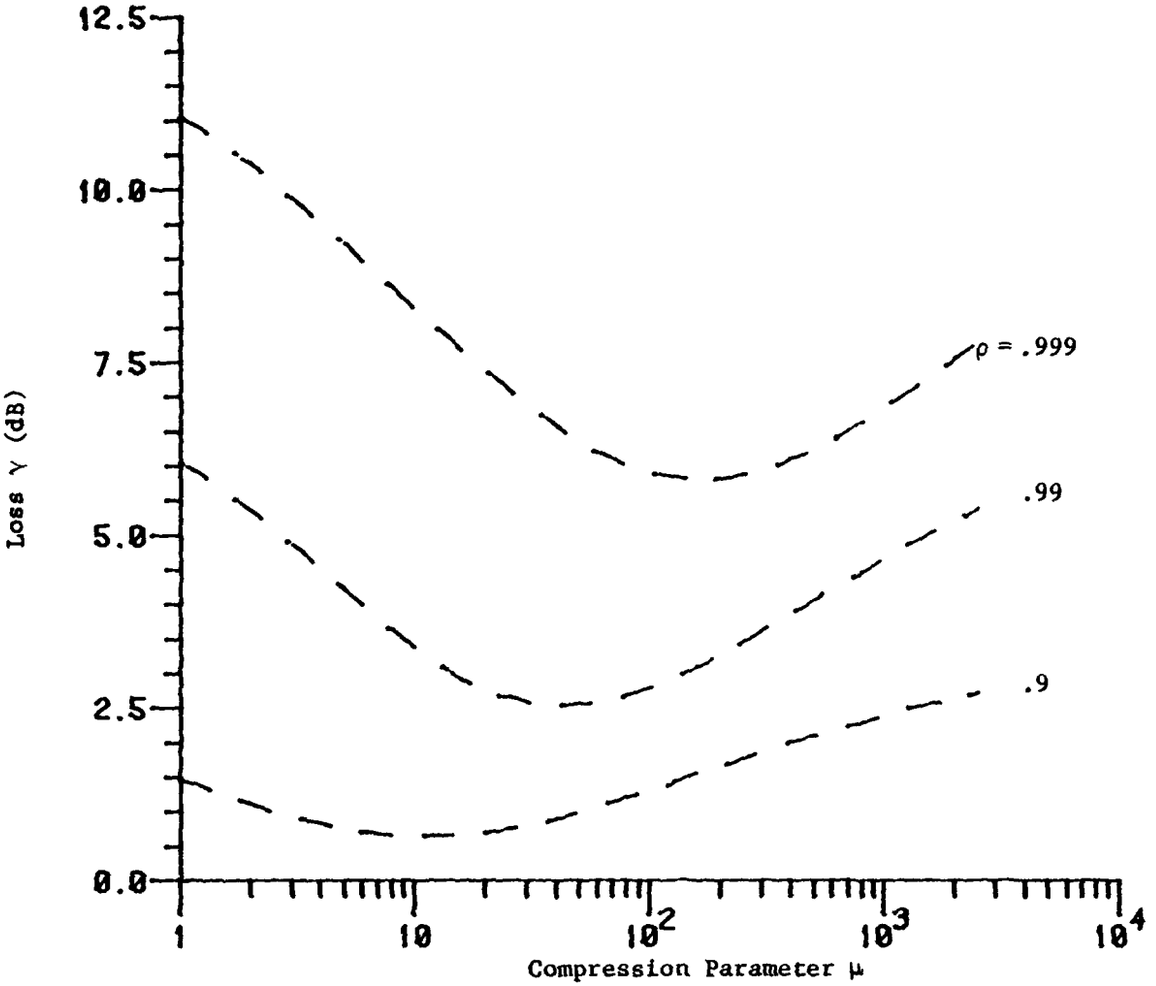


Figure 4.9. Loss of single canceller MTI with 32-level μ-law quantizer and V = 10.

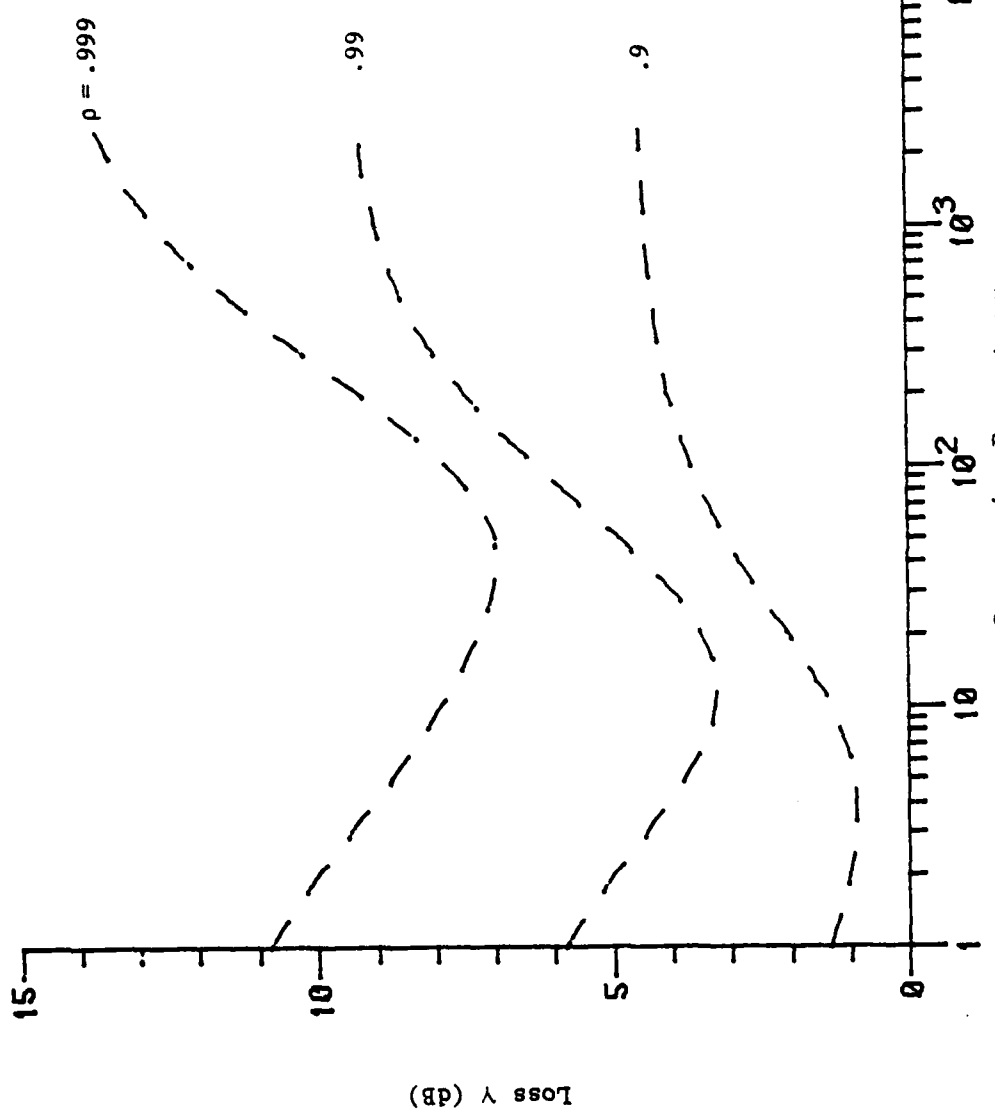


Figure 4.10. Loss of single canceller MTI with 8-level μ-law quantizer and V = 1000.

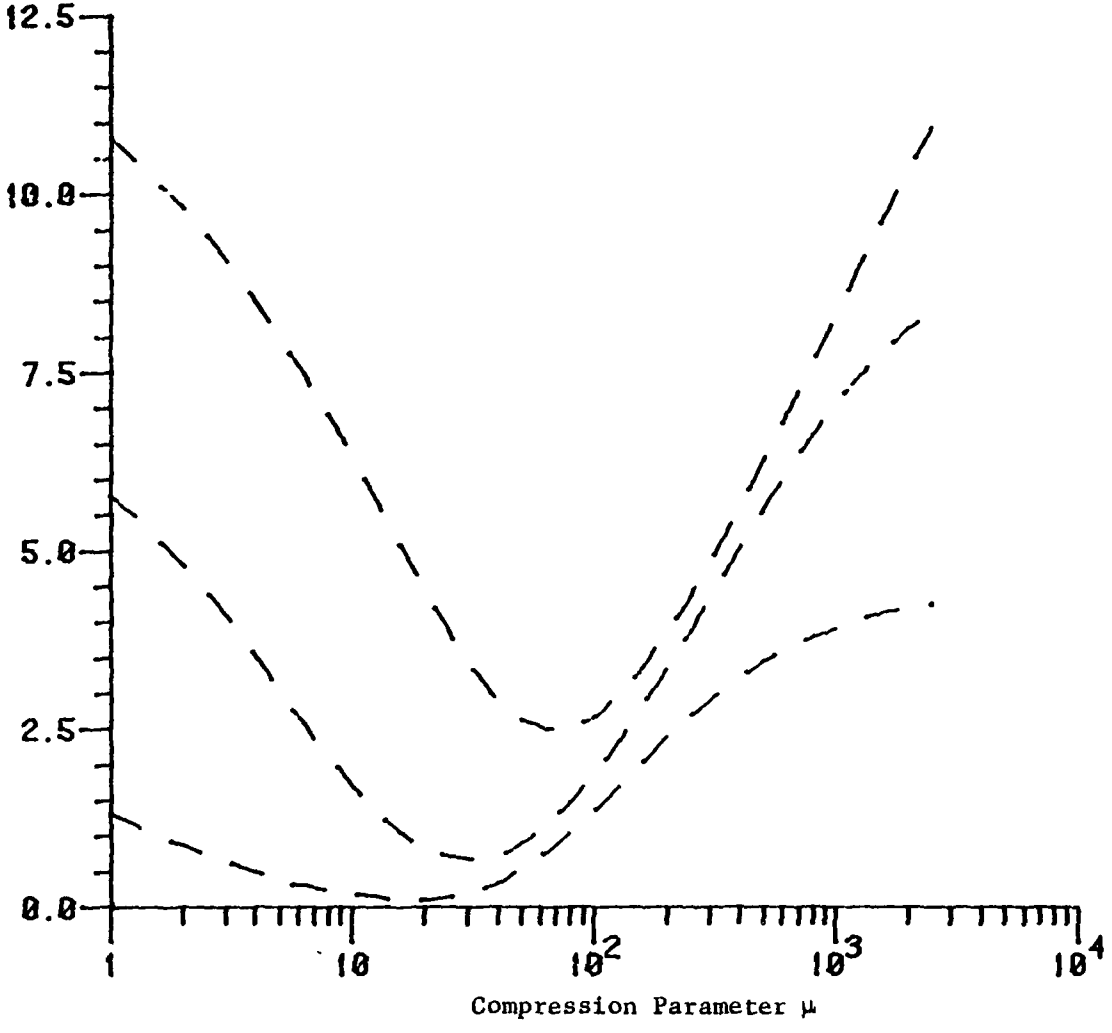


Figure 4.11. Loss of single canceller MTI with 32-level μ-law quantizer and V = 1000.

Table 4.3. Single canceller MTI with $\mu$-law quantizer for optimum $\mu$ and minimum loss $\gamma$ V = 10.

| $\rho_x$ | .9 | | .99 | | .999 | |
|---|---|---|---|---|---|---|
| Number of Levels | Optimum $\mu$ | Minimum Loss (dB) | Optimum $\mu$ | Minimum Loss (dB) | Optimum $\mu$ | Minimum Loss (dB) |
| 4 | 1.7 | 2.14228326 | 10.0 | 5.73871619 | 44.0 | 10.138973 |
| 8 | 5.6 | .89340755 | 21.0 | 3.30004448 | 79.0 | 7.07642609 |
| 16 | 11.0 | .64119459 | 42.0 | 2.54243282 | 159.0 | 5.8119278 |
| 32 | 11.0 | .64119447 | 42.0 | 2.54241816 | 165.0 | 5.81134206 |

Table 4.4. Double canceller MTI with $\mu$-law quantizer for optimum $\mu$ and minimum loss $\gamma$ V = 10.

| $\rho_x$ | .9 | | .99 | | .999 | |
|---|---|---|---|---|---|---|
| Number of Levels | Optimum $\mu$ | Minimum Loss (dB) | Optimum $\mu$ | Minimum Loss (dB) | Optimum $\mu$ | Minimum Loss (dB) |
| 4 | 2.50 | 6.17410368 | 18.0 | 19.1857495 | 93.0 | 33.69662710 |
| 8 | 7.4 | 3.28242898 | 50.0 | 14.9618675 | 253.0 | 29.6168799 |
| 16 | 13.9 | 2.55638117 | 86.0 | 14.2535857 | 414.0 | 28.8994491 |
| 32 | 13.9 | 2.55637348 | 87.0 | 14.2534183 | 419.0 | 28.893708 |

ii) Double Canceller MTI

Figure 4.12 shows the loss as related to $\rho$ which goes from 0.1 to 0.999. The loss curves here produce the same trend as those obtained for the single canceller MTI, but the loss grows much higher than the single canceller case. Figures 4.13 and 4.14 show the loss as a function of $\mu$ with 8 and 32 level quantizers for the case V = 10. It is seen that the loss is insensitive to the value of $\mu$ chosen since each curve is rather flat as compared to that of the single canceller case. When V is increased to 1000, the loss curves are done over and the data is plotted in Figs. 4.15 and 4.16. Here the loss becomes more sensitive to the value of $\mu$. For all the figures shown, an optimum $a_k$ can always be found. Finally, more quantizer levels and larger preset input voltage are favorable towards the optimum performance of a double canceller MTI. Again, there is always a limit on the loss here. Table 3.4 lists the optimum $\mu$'s and their loss with V = 10 for values of M ranging from 4 to 64.

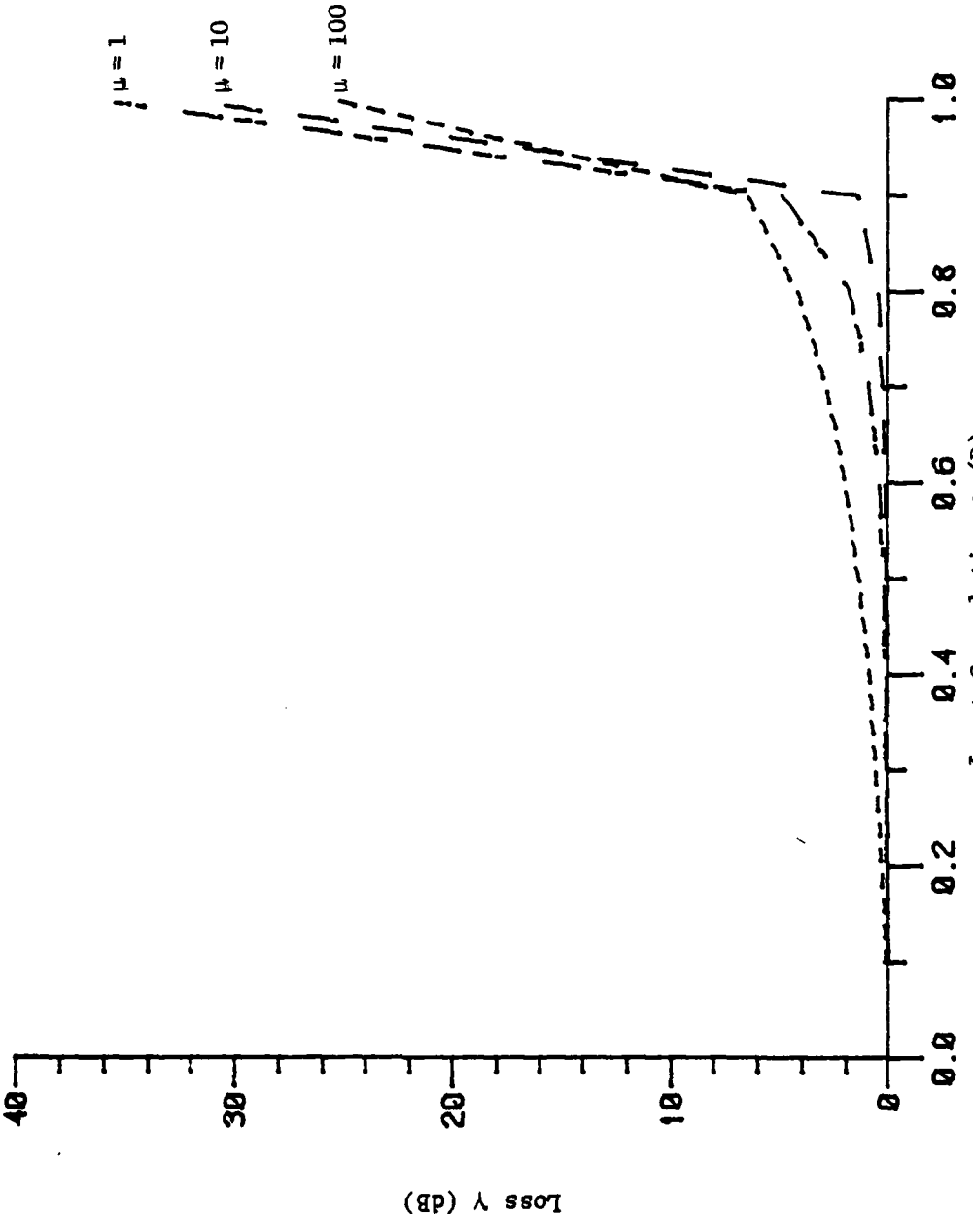


Figure 4.12. Loss of double canceller MTI with 16-level μ-law quantizer and V = 100.

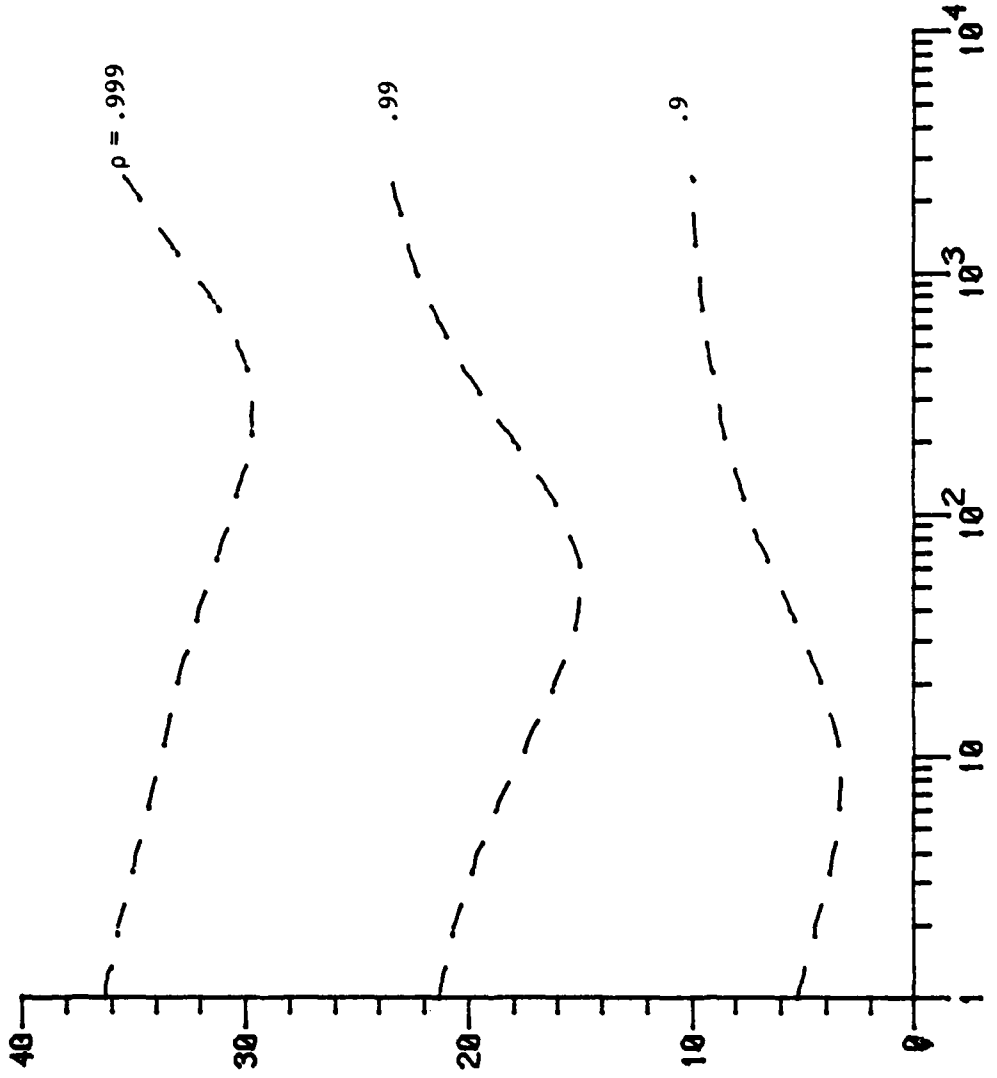


Figure 4.13. Loss of double canceller MTI with 8-level μ-law quantizer and V = 10.

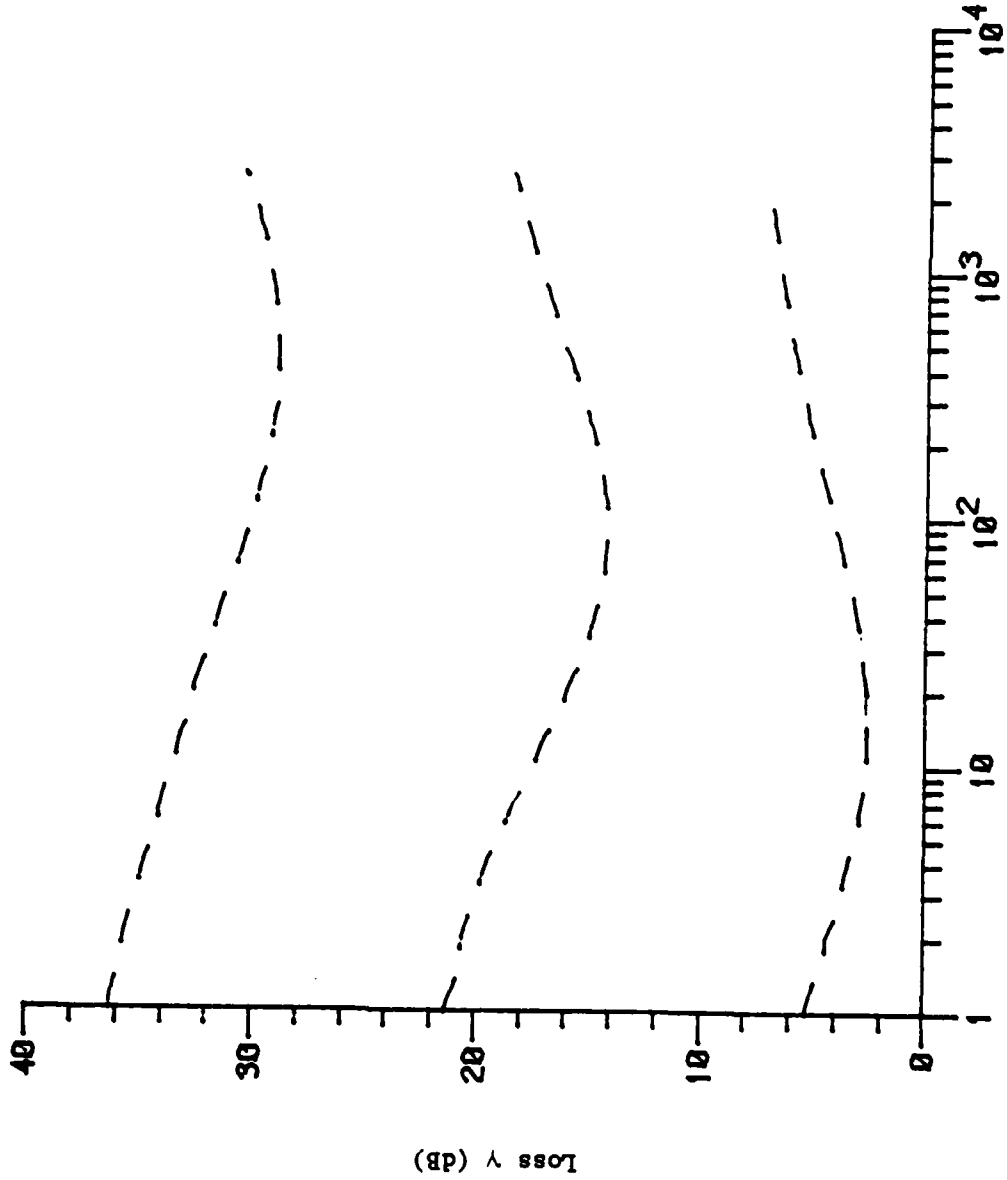


Figure 4.14. Loss of double canceller MTI with 32-level μ-law quantizer and V = 10.

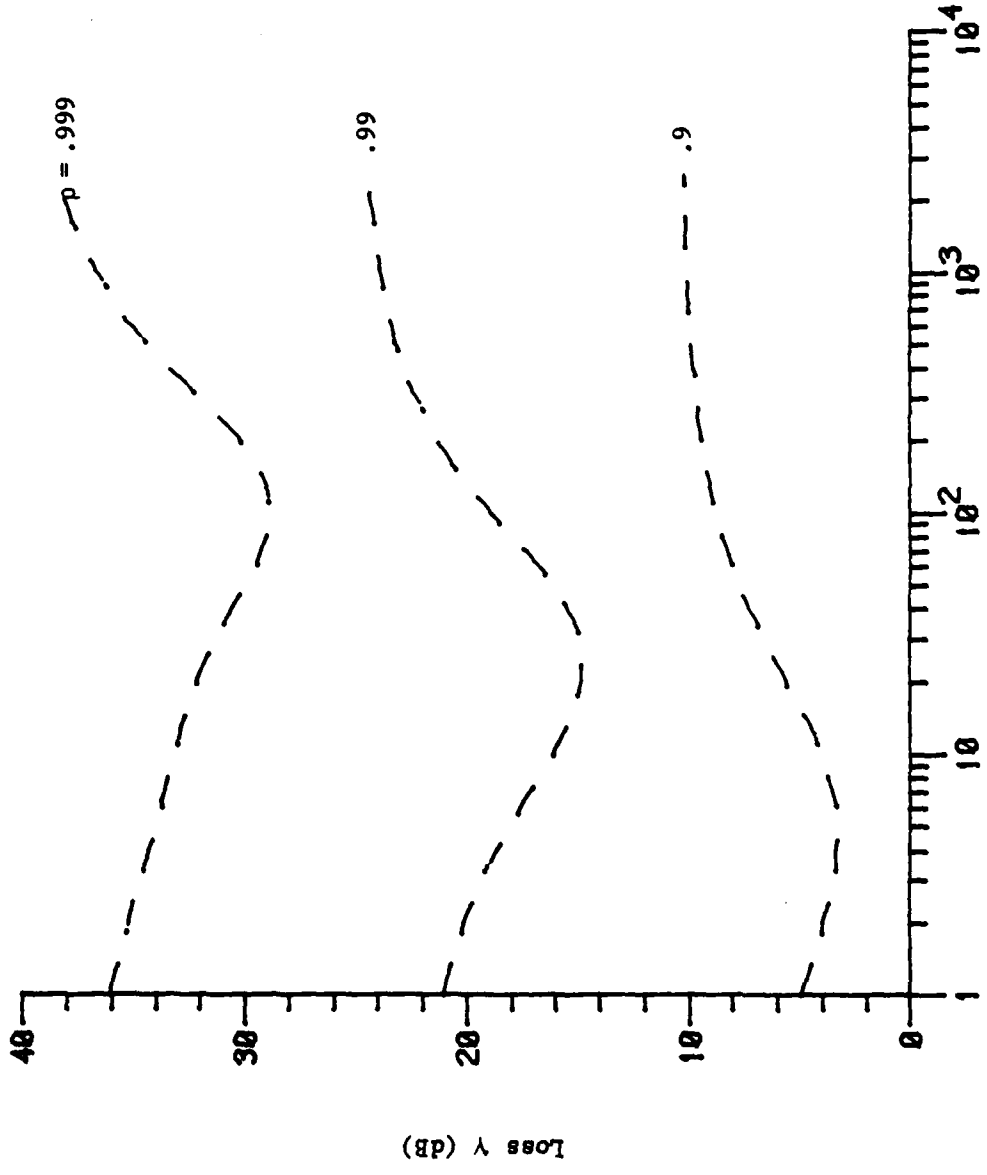


Figure 4.15. Loss of double cancellar MTI with 8-level μ-law quantizer and V = 1000.

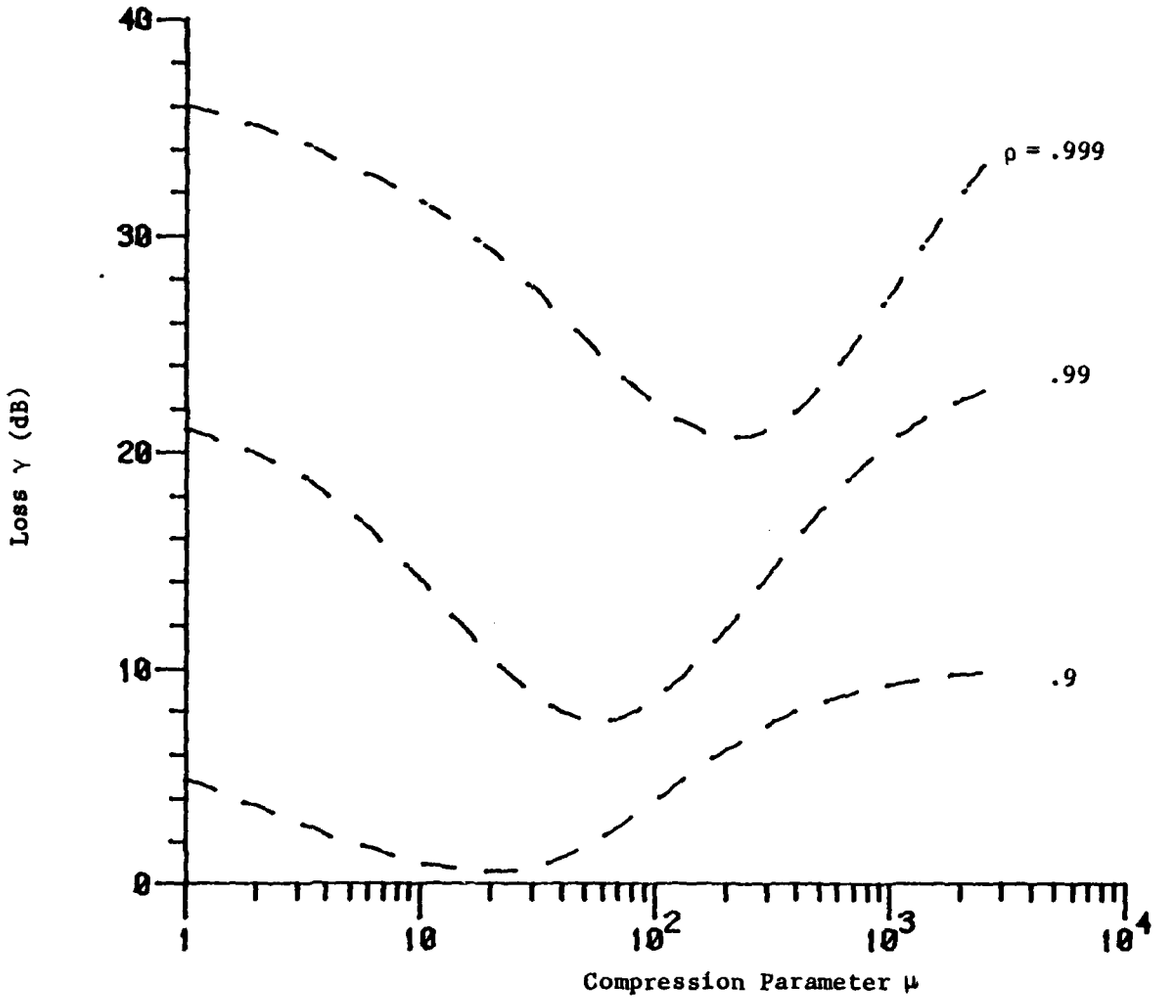


Figure 4.16. Loss of double canceller MTI with 32-level μ-law quantizer and V = 1000.

# 5. CONCLUSIONS

It has been shown that quantization effects on digital moving target indication depend on the number of output quantization levels and the spacing of these levels. Among the quantizers discussed before, the clutter attenuation is being used as the performance criterion. It has been shown that, in general, uniform, logarithmic and $\mu$-law quantizers give almost identical performance for a few quantizer levels. As a matter of fact, a 4-level uniform quantizer is equivalent to a 4-level logarithmic quantizer. As the number of quantizer levels increases, the uniform quantizer gives the best performance and logarithmic quantizer presents the worst. However, as the comparison parameter approaches zero, a $\mu$-law quantizer will be similar to a uniform quantizer. Moreover, it is likely to happen that, with a large enough number of output levels, the loss will not be improved by any significant amount. Hence, it is concluded that the uniform quantizer is the best fitted in the sense that the performance of digital MTI using the uniform quantizer gives a minimum loss corresponding to an optimum spacing, under the assumptions that the input clutter process is Gaussian and the quantizer has uniform step size. Finally, it has been verified that there exists a common bound on the loss for uniform, logarithmic and $\mu$-law quantizers.

It was seen that, in general, uniform, logarithmic and $\mu$-law quantizers give almost identical performance at few quantizer levels. As a matter of fact, a 4-level uniform quantizer is equivalent to a 4-level logarithmic quantizer. As the number of quantizer levels increases, uniform quantizer gives the best performance and logarithmic

quantizer presents the worst. However, as the compression parameter approaches zero, a $\mu$-law quantizer will be similar to a uniform quantizer. Moreover, it is likely to happen that, with a large enough number of output levels, the loss will not be improved by any significant amount.

REFERENCES

[1] D. L. Barton, Radar System Analysis, Prentice-Hall, Englewood cliffs, N. J., 1964.

[2] R. C. Emerson, "Some pulsed Doppler MTI and AMTI Techniques," Rand Corporation Rept. R-274, pp. 1-124, March 1954.

[3] W. D. White and A. E. Ruvin, "Recent advances in the synthesis of comb filters," IRE Natl. Conv. Record, vol. 5, part 2, pp. 186-200, 1957.

[4] H. Urkowitz, "Analysis and synthesis of delay line periodic filters," IRE Transactions on Circuit Theory, vol. CT-4, no. 2, pp. 41-53, June 1957.

[5] D. A. Linden and B. D. Steinberg, "Synthesis of delay line networks," IRE Transactions on Aeronautical and Navigational Electronics, vol. ANE-4, no. 1, pp. 34-39, March 1957.

[6] J. Capon, "Optimum weighting functions for the detection of sampled signals in noise," IEEE Transactions on Information Theory, vol. IT-10, no. 2, pp. 152-159, April 1964.

[7] L. E. Brennan and I. S. Reed, "Optimum processing of unequally spaced radar pulse trains for clutter rejection," IEEE Transactions on Aerospace and Electronic Systems, vol. AES-4, no. 3, pp. 474-477, May 1978.

[8] J. K. Hsiao, "On the optimization of MTI clutter rejection," IEEE Transactions on Aerospace and Electronic Systems, vol. AES-10, no. 5, pp. 622-629, September 1974.

[9] D. C. Schleher and D. Schulkind, "Optimization of nonrecursive MTI," IEE International Radar Conference, London, pp. 182-185, October 1977.

[10] R. McAulay, "A theory for optimal moving target indication (MTI) digital signal processing (Supplement 1)," MIT Lincoln Laboratory pp. 1-16, October 31, 1972.

[11] F. Dickey, "Theoretical performance of airborne moving target indicators," IRE Transactions on Aeronautical and Navigational Electronics, PGAE-8, pp. 12-23, June 1953.

[12] R. E. Hendrix, "Overland downlook radar is key element of AWACS," Westinghouse Engineer, vol. 33, no. 4, pp. 98-105, July 1973.

[13] T. ap Rhys and G. Andrews, "AEW radar antennas," AGARD Conference Preprint no. 139, Antennas for Avionics, pp. 12-1 - 12-16, 1974.

[14] W. Szajnowski, "The generation of correlated Weibull clutter for signal detection problems," IEEE Transactions on Aerospace and Electronic Systems, vol. AES-13, no. 5, pp. 536-540, September 1977.

[15] P. S. Tong, "Quantization requirements in digital MTI," IEEE Transactions on Aerospace and Electronic Systems, vol. AES-13, no. 5, pp. 512-521, September 1977.

[16] L. E. Brennan and I. S. Reed, "Quantization noise in digital moving target indication systems," IEEE Transactions on Aerospace and Electronic Systems, vol. AES-2, pp. 655-658, November 1966.

[17] H. R. Ward and W. W. Shrader, "MTI performance degradation caused by limiting," EASCON Tech. Conv. Rec., pp. 168-174, 1968.

[18] R. F. Baum, "The correlation function of smoothly limited Gaussian noise," IRE Transactions on Information Theory, vol. IT-3, pp. 193-197, September 1957.

[19] G. Grasso, "Improvement factor of a nonlinear MTI in point clutter," IEEE Transactions on Aerospace and Electronic Systems, vol. AES-4, pp. 640-644, July 1968.

[20] A. I. Velichkin, "Correlation function and spectral density of a quantized process," Telecommunications and Radio Engineering, pt. 2: Radio Engineering, pp. 70-77, July 1962.

[21] J. F. Barrett and D. G. Lampard, "An expansion for some second-order probability distributions and its application to noise problems," IRE Transactions on Information Theory, vol. IT-1, pp. 10-15, March 1955.

[22] H. Cramér, Mathematical Methods of Statistics, Princeton University Press, Princeton, N.J., 1946, p. 133.

[23] J. H. Van Vleck and D. Middleton, "The spectrum of clipped noise," Proceedings of IEEE, vol. 54, pp. 2-19, January 1966.

[24] P. E. Panter and W. Dite, "Quantizing distortion in pulse-count modulation with nonuniform spacing of levels," Proceedings of IRE, vol. 39, pp. 44-48, 1951.


FILM
8